

Machine-Learning Dessins d’Enfants: Explorations via Modular and Seiberg-Witten Curves

Yang-Hui He^{1,2,3*}, Edward Hirst^{1†}, Toby Peterken^{4‡}

July 12, 2022

¹ *Department of Mathematics, City, University of London, EC1V 0HB, UK*

² *Merton College, University of Oxford, OX1 4JD, UK*

³ *School of Physics, NanKai University, Tianjin, 300071, P.R. China*

⁴ *Keble College, University of Oxford, OX1 3PG, UK*

Abstract

We apply machine-learning to the study of dessins d’enfants. Specifically, we investigate a class of dessins which reside at the intersection of the investigations of modular subgroups, Seiberg-Witten curves and extremal elliptic K3 surfaces. A deep feed-forward neural network with simple structure and standard activation functions without prior knowledge of the underlying mathematics is established and imposed onto the classification of extension degree over the rationals, known to be a difficult problem. The classifications exceeded 0.93 accuracy and around 0.9 confidence relatively quickly. The Seiberg-Witten curves for those with rational coefficients are also tabulated.

*hey@maths.ox.ac.uk

†edward.hirst@city.ac.uk

‡toby.peterken@keble.ox.ac.uk

Contents

1	Introduction & Summary	2
2	Dramatis Personnae	4
2.1	dessins d'enfants	4
2.1.1	Belyi's Theorem and Graph Theory	4
2.1.2	Dessin Transformations and Galois Representation	7
2.2	Modular K3 Surfaces	8
2.2.1	Subgroups of the Modular Group $PSL(2, \mathbb{Z})$	8
2.2.2	Dessins from j -maps	9
2.3	The Dessin Database	11
2.4	Seiberg-Witten Theory	12
2.4.1	Sieberg-Witten Curves	12
2.4.2	Dessins to Seiberg-Witten Curves	14
3	Classifying the Dessin Extensions	15
3.1	Data Engineering	15
3.2	Setup of the Machine-Learning Model	17
3.3	NN Results	18
4	Conclusion & Outlook	21
A	Reproducing the Riemann Surface	22
B	Generated Seiberg-Witten Curves	23
C	The Dessin d'Enfant Dataset	28

1 Introduction & Summary

Alexander Grothendieck's Dessins d'enfants, or childrens' drawings, laid a cornerstone of modern mathematics, inspiring a confluence of geometry, combinatorics, and number theory. Having learnt of the remarkable theorem of Belyi [1] which relates the existence of algebraic models of Riemann surfaces to that of analytic properties of rational functions thereon, Grothendieck launched an entire programme [2] by pictorially representing¹ this structure as bipartite graphs (the dessin) drawn on the Riemann surface. He hypothesised dessins d'enfants in their current form as a conceptual representation of the absolute Galois group over the rationals, one the most mysterious and least understood objects in number theory. Subsequently, he developed a generalisation of Belyi's theorem which extends the surfaces considered in the mapping to more general Riemann surfaces. Properties of the mapping are identified with combinatorial invariants of the dessin d'enfant graphs [2] (q.v. several standard introductory books and lecture notes in [4, 5, 6, 7]).

Remarkably, this beautiful story has more recently found its place in theoretical physics, especially in supersymmetric gauge theories and string theory. These have ranged from a novel way of factorizing [8] Seiberg-Witten curves [9], to realizing [10, 11, 12] brane-tilings and dimer models, which is the most general method [13] of understanding $\text{AdS}_5/\text{CFT}_4$ for toric Calabi-Yau spaces, as well as to certain elliptic K3-surfaces [14] and their relation [15] to generalized quiver gauge theories [16].

One downside to the *esquisse* is that Belyi maps are notoriously difficult to compute explicitly: whilst the dessin is easy to draw, the underlying map to the Riemann sphere could very quickly involve algebraic numbers unimaginable from the shape of the graph. To give an example from physics, the brane-tiling/dessin for the so-called suspended pinched point Calabi-Yau singularity had been known for a decade [13] and consists of a simple triangle-rectangle tessellation of the doubly-periodic plane, but it took years [17] to construct the Belyi map as a rational function. Indeed, as always, Grothendieck's power lies in the profundity of an abstract panorama, rather than in the mundanity of computation and untidy expressions.

Recently, a paradigm was established to see whether the latest techniques in machine-learning (ML) and data science can be used to study mathematical structures, and in particular, whether otherwise prohibitive calculations could be bypassed, at least stochastically [18]. Indeed, [18, 19, 20, 21] brought about machine-learning to string/gauge theory (see [22, 23, 24] and references therein for reviews). Various problems in mathematics and theoretical physics have been put to the test by neural-networks and classifiers with architectures without a priori knowledge of the underlying mathematical structures.

An intuitive hierarchy of difficulty is beginning to emerge [25]: numerical algorithms such as those finding Calabi-Yau volumes [19] and Ricci-flat metrics [26] seem most amenable to ML, slightly less behaved though oftentimes comparable in performance are problems in

¹Interestingly, F. Klein had the vision, when considering a 11-fold cover of the Riemann sphere, to draw a diagram which he called *Linienzüge* (line-tracks) [3], which is really a prototype for a dessin.

algebraic geometry over \mathbb{C} such as topological invariants and bundle cohomology [18, 20, 21, 27, 28]. Luckily for string theory, these two classes of problems are the most typical ones encountered. At the next level of difficulty are algebraic and combinatorial problems, such as determining the simplicity of finite groups [29] and property of graphs [30, 31]. The very zenith of complexity, as expected, is number theory. To have a neural network predict the next prime, for instance, would be unfathomable: indeed simple experiments in [18] showed that the AI is doing no better than randomly guessing. Yet, problems in number theory are still within the grasp of algebraic geometry and analysis seems to be slightly better than random guesses: the archetypal problem, the Birch-Swinnerton-Dyer conjecture, was subject to various ML algorithms in [32] and found to be so.

It is therefore natural to question, uniting our above two strands of thought, how the discipline of dessins d’enfants, overarching algebraic geometry, graph theory and algebraic number theory, responds to ML. Given the paucity of available data - in part due to the aforementioned difficulty of computing Belyi maps - it is a challenge to find a suitable dataset on which we could try supervised and unsupervised machine-learning. Fortunately, a convenient set of dessins has been established in the literature, with the added bonus of involving some further elegant mathematics and physics. Simultaneously exploiting the method of [8] which related dessins to Seiberg-Witten curves, that of [33, 34] in recognizing that the j -invariant of elliptic K3-surfaces are Belyi, as well as that of [35, 36] in representing the Cayley coset graph of congruence subgroups of the modular group $PSL(2, \mathbb{Z})$ as bipartite graphs (and hence to $\mathcal{N} = 2$ generalized quiver theories [15, 37]), [14] focused on a set of 112 distinguished K3 surfaces, the so-called extremal ones.

These K3 surfaces of concern are elliptically fibred over \mathbb{P}^1 so the j -invariant of the fibering elliptic curves are naturally a rational function $j(z)$ of the base projective coordinate of \mathbb{P}^1 . Interestingly, $j(z)$ is a Belyi map onto the base Riemann sphere and gives a dessin d’enfant. Most of these have been determined explicitly [34], and at least the extension-degree over \mathbb{Q} for all of them are computed. Meanwhile, the monodromy group of the covering of \mathbb{P}^1 (equivalently, the cartographic group of the dessin) were computed in [14]. We will therefore take a two-pronged approach in this paper. First, we complete the task of [15] (wherein 33 special cases of the 112, corresponding to torsion-free congruence subgroups of $PSL(2, \mathbb{Z})$ were translated to Seiberg-Witten curves) and provide the full correspondence of modular-subgroup/elliptic K3 surface/dessins/Seiberg-Witten curves for the 112 extreme K3 surfaces.

Second, and this is a much more curious and potentially very useful direction, we ask the question: *can aspects of dessins be machine-learnt?* Specially, we can ask the following simple classification problem to a neural network (NN) with no knowledge of mathematics: given the dessin, drawn as a bipartite graph on a plane, there is an intrinsic integer, viz., the transcendence degree over \mathbb{Q} , which is crucial to the underlying number theory and which is difficult to obtain; can this degree be learned by training the NN in a supervised way?

The purpose of this paper is to address these two directions. The Seiberg-Witten curves can be found algorithmically and are tabulated in appendix B. Surprisingly, a relatively simple deep-feed-forward NN, which takes the adjacency matrix of the dessin as input and the transcendence degree as output, can reach accuracy in the 90%’s rather quickly. This

suggests the possibility of a way to directly understand the Galois orbits of dessins, and thence the absolute Galois group, from the adjacency of the graphs, at least stochastically.

The paper is structured to provide an introduction to the dessin d'enfant graphs in sections §2.1 and §2.2; explaining their importance in the Galois theory context, and their relation to Calabi-Yau manifolds in the context of algebraic geometry and string theory. Next, the mechanism of producing Seiberg-Witten curves, motivating the study of dessins for considering physical theories in the IR limit, is presented in section §2.4. Following this the analysis of the machine-learning methods to classify the dataset are given in section §3. The results show success in identifying a dessin's extension degree from its adjacency matrix. The appendices provide further discussion of the Belyi pair - dessin equivalence, and list both the full dataset of dessins analysed, and the corresponding Seiberg-Witten curves.

2 Dramatis Personnae

We begin with a rapid introduction of the various ingredients from the mathematics and the physics, highlighting in a data-base of dessins denfants which will be central to our analysis.

2.1 dessins d'enfants

2.1.1 Belyi's Theorem and Graph Theory

Let X be a smooth, compact, connected Riemann surface. A remarkable theorem [1] states that

Theorem 2.1 (Belyi). *X has an algebraic model over $\overline{\mathbb{Q}}$ IFF there exists a (surjective) map $\beta : X \rightarrow \mathbb{P}^1$ which is ramified at exactly 3 points.*

The covering map β has come to be known as a **Belyi Map**. The depth of this theorem stems from the following. We know that a Riemann surface of genus g , as an algebraic variety, can be written, for example, as a hyper-elliptic curve², i.e., as a polynomial of degree $2g + 1$ (or $2g + 2$) in \mathbb{C}^2 with coordinates (x, y) . The coefficients in this polynomial dictate the complex structure and in principle could be arbitrary complex numbers. Belyi's theorem tells us that IFF one can find a rational map $\zeta = \beta(x, y)$ from X to \mathbb{P}^1 with coordinate ζ which is ramified (not 1-1) at precisely 3 points, then the complex coefficients are algebraic numbers [4].

Now, by Möbius transformation $\zeta \mapsto \frac{a\zeta + b}{c\zeta + d}$, for $a, b, c, d \in \mathbb{C}$ on the coordinate ζ of \mathbb{P}^1 , any 3 generic points can be taken to $(0, 1, \infty)$. In other words, Belyi's theorem dictates

²We should, of course, include the point at infinity by projectivising \mathbb{C}^2 to \mathbb{P}^2 but for convenience, we will work in the affine patch with ordinary coordinates (x, y) and remember to include (∞, ∞) explicitly.

that IFF we can find a rational function $\beta(x, y)$ on X at whose pre-images for 0, 1 and ∞ the Taylor series after the constant term (which is, of course, 0, 1, or ∞ respectively) starts at an order $n > 1$, then X has complex structure over $\overline{\mathbb{Q}}$. The positive integer n is called the **ramification index**.

We emphasize that β is a covering map and thus highly surjective in that there could be an arbitrary number of pre-images of $(0, 1, \infty)$ and we need to perform Taylor series at all of these pre-images. We can collect all the ramification indices into a so-called **passport**, which is the list of ramification indices for each of these pre-images of 0, 1, and ∞ . Grothendieck's insight was to realize that the Belyi map gives an embedded graph on X as follows:

Definition 2.1. Consider $\beta^{-1}(0)$, which is a set of points on Σ that can be coloured as white, and likewise $\beta^{-1}(1)$, black. The pre-image of any simple curve with endpoints 0 and 1 on \mathbb{P}^1 is a bipartite graph embedded in Σ whose valency at a point is given by the ramification index (i.e., order of vanishing of Taylor series) on β . This is the **dessin d'enfant**.

Restricted by Riemann-Hurwitz, $\beta^{-1}(\infty)$ is not an independent degree of freedom, but is rather taken 1-to-1 to the faces in the bipartite graph, with the number of sides of the polygonal face being twice the ramification index. The passport can then be written as

$$[r_0(1), r_0(2), \dots, r_0(B) \mid r_1(1), r_1(2), \dots, r_1(W) \mid r_\infty(1), r_\infty(2), \dots, r_\infty(I)] , \quad (2.1)$$

where $r_0(j)$ is the valency (ramification index) of the j -th white node, likewise $r_1(j)$, that for the j -th black node, and $r_\infty(j)$, half the number of sides to the j -th face. The passport does not uniquely determine it since one further needs the connectivity between the white/black nodes, but it is nevertheless an important quantity. The *degree* of the Belyi map is the row-sum $d = \sum_j r_0(j) = \sum_j r_1(j) = \sum_j r_\infty(j)$ and is the degree of β as a rational function. The collection of (X, β) gives the *Belyi pair* which can be used to represent a dessin.

Throughout this paper we will only be concerned with genus zero or **planar dessins**. That is, the Belyi maps will be from $X = \mathbb{P}^1$ (with coordinate z) to \mathbb{P}^1 (with coordinate ζ) and will be a rational function in a single complex variable. That is,

$$\zeta = \beta(z) = P(z)/Q(z) : \mathbb{P}_z^1 \rightarrow \mathbb{P}_\zeta^1 \quad (2.2)$$

with polynomials $P(z)$ and $Q(z)$.

The dessins considered in this study are also **clean** as well as planar, such that the degree of all black vertices is 2, these are the pre-images of 1. Of course, which colour we choose for pre-images of 0 or 1 is purely by convention and we adhere to that of colouring pre-images of 0 and 1 as white and black respectively. Moreover, 0, 1 and ∞ can be transformed freely amongst themselves by $SL(2; \mathbb{C})$ so we need to fix a convention for β from the start as well.

An example of a clean planar dessin is given in figure 1; this will be our running example in this section and the various mathematical and physical structures described in this paper will be explicitly shown as we proceed with this introduction.

The passport is $\begin{Bmatrix} 3^8 \\ 2^{12} \\ 4^6 \end{Bmatrix}$, where 3^8 means there are 8 white nodes of valency 3, 2^{12} means there are 12 black nodes of valency 2 (this means that the dessin is clean in that all of one colour have valency 2). Finally, the 4^6 means that there are 6 faces - note that we are drawing on $\mathbb{P}^1 \simeq S^2$ so there is a point at infinity for which there is an exterior face in addition to the 5 visible ones. The triangulation of the dessin faces leads to a list of number of triangles for each face which is exactly twice each entry of the passport. Of course, this example dessin is precisely the cube, drawn on a sphere.

The Belyi pair corresponding to this dessin can be reproduced, and the mapping to \mathbb{P}^1 gives the Belyi function up to biholomorphism. Choosing a version equivalent to the Belyi map provided in [38], we see that this dessin's Belyi map is:

$$\beta(z) = \frac{(z^8 - 14z^4 + 1)^3}{(-108z^4(z^4 + 1)^4)}, \quad (2.3)$$

noting that this Belyi map differs to the map provided in [36] by a birational transformation. Calculating the preimages of $\{0, 1, \infty\}$ under (2.3), the dessin in figure 1 can be reproduced. The preimages of 0 correspond to roots of the Belyi map numerator. The preimages of 1 correspond to roots of the polynomial formed from the difference of the Belyi map numerator and denominator. Finally the preimages of ∞ are given by the limit $z \mapsto \infty$, or the roots of the Belyi map denominator. Furthermore, the ramification at preimage z_0 is the leading order of the Taylor series of $\beta(z)$ at z_0 . In summary: In each case the number of preimages

Images $\beta(z)$	Preimages z	No. of Preimages	Ram. Ind.
0	$\sqrt{2 \pm \sqrt{3}}, -\sqrt{2 \pm \sqrt{3}}, i\sqrt{2 \pm \sqrt{3}}, -i\sqrt{2 \pm \sqrt{3}}$	8	3
1	$\pm 1, \pm i, \pm \left(1 + \frac{1}{\sqrt{2}} + i\sqrt{\frac{1}{2}(3 + 2\sqrt{2})}\right), \pm \left(1 + \frac{1}{\sqrt{2}} - i\sqrt{\frac{1}{2}(3 + 2\sqrt{2})}\right), \pm \left(1 - \frac{1}{\sqrt{2}} + i\sqrt{\frac{1}{2}(3 - 2\sqrt{2})}\right), \pm \left(1 - \frac{1}{\sqrt{2}} - i\sqrt{\frac{1}{2}(3 - 2\sqrt{2})}\right)$	12	2
∞	$0, \pm \frac{1}{\sqrt{2}}(1 + i), \pm \frac{1}{\sqrt{2}}(1 - i), \infty$	6	4

Table 1: The preimages of $\{0, 1, \infty\}$, along with their multiplicities, for a Belyi map corresponding to congruence modular subgroup $\Gamma(4)$.

and the multiplicities agree with this example dessin's passport. Therefore producing the 8 trivalent white vertices, 12 bivalent black vertices, and 6 faces (including the outer face) of the dessin in this example.

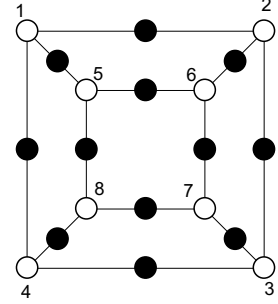


Figure 1: An example of a dessin d'enfant. This dessin is of the type examined in this paper, it is a planar dessin, and also clean - hence only the white vertices are labelled.

2.1.2 Dessin Transformations and Galois Representation

It is through Belyi's theorem that dessins provide the surface they are embedded in with an obvious Riemann structure, since through interpretation of the dessin, the surface X can be described via algebraic curves with coefficients as algebraic numbers. The key to Grothendieck's *Esquisse* is that the combinatorial interpretation of dessins d'enfants is related to the absolute Galois group over the algebraic rational numbers. This group describes how these algebraic curves (and hence dessins also) transform into each other [6]. This interpretation of dessins d'enfants is as an object to represent the combinatorial invariants associated with the action of the **absolute Galois group**³ of the rational numbers, $Gal(\overline{\mathbb{Q}}/\mathbb{Q})$. The group $Gal(\overline{\mathbb{Q}}/\mathbb{Q})$, has no direct description, it is hence through Belyi's theorem that dessin d'enfant graphs become of interest, to study this group [7, 40].

The important relation which the theory of dessins capitalises on is an equivalence between several categories. The equivalence relates the category of embedded dessin graphs with: finite sets under permutation; field extensions; and certain types of algebraic curves. Since field extensions are directly related to the definition of the absolute Galois group, it is through this categorical equivalence that representations of the Galois group act *faithfully* on dessins d'enfants. This is what makes dessins so useful in studying the elusive $Gal(\overline{\mathbb{Q}}, \mathbb{Q})$ group.

Triangulation of the dessin allows the original Riemann surface's algebraic curve from the Belyi pair to be reproduced up to homeomorphism. This process is further explained in appendix A. This triangulation process also directly demonstrates the category equivalence to finite sets under permutation, by defining reflection operators over the triangles produced.

Reconsidering the absolute Galois group, action of its elements may change the subfields of the algebraic completion which the Belyi functions are defined over, this maps Belyi pairs to each other, and hence corresponds to this mapping within orbits of dessins. The orbit of a dessin is all dessins that the absolute Galois group can transform the original dessin into. The largest orbit in the dataset we consider corresponds to a quartic extension of the rationals, as shown in appendix C corresponding to passport: 12-5-3-2-1-1. The minimal polynomial associated with the quartic root used in the extension hence has 4 distinct roots (since the extension is also separable). Therefore each dessin in this Galois orbit corresponds to an extension of the rationals by one of these 4 roots. The root corresponding to each of these dessins is used in defining the coefficients of its Belyi map.

The dessins therefore act as tools to identify invariants and other properties of the rational absolute Galois group. Invariants such as degree sequence (the list of vertex degrees), and the stabiliser of the orbit act as important insights from the theory of dessins into study

³In defining the Galois group, *Galois extensions* of a base field are considered. These are algebraic field extensions which are both normal, and separable [39, 40]. A Galois group is then the group of all automorphisms of a Galois extension which fix the base field. Beyond these the *absolute* Galois group of a field, requires a specific extension of the base field known as the separable closure of the field. Note that since the base field considered, \mathbb{Q} , is perfect, the separable closure is equal to its algebraic closure denoted $\overline{\mathbb{Q}}$.

of this group [6]. Importantly the size of the orbit of a dessin corresponds to the degree of the field extension, and it is classification according to this degree which machine-learning is used for in this study.

2.2 Modular K3 Surfaces

Having introduced dessins, let us move on to two seeming unrelated subjects: subgroups of $PSL(2, \mathbb{Z})$ and K3 surfaces. It is remarkable that they both give rise to dessins.

2.2.1 Subgroups of the Modular Group $PSL(2, \mathbb{Z})$

Consider the modular group $\Gamma = PSL(2, \mathbb{Z})$, which is an infinite group generated by two elements $\Gamma := \langle S, T | S^2 = (ST)^3 = I \rangle$. The most familiar subgroup is the principal congruence subgroup⁴

$$\Gamma(m) := \{A \in \Gamma : A = I \pmod{m}\}. \quad (2.4)$$

A principal congruence subgroup of *level* m is one which contains $\Gamma(m)$ but not $\Gamma(n)$ for any $n < m$. There are more exotic congruence subgroups of Γ defined by modulo operations such as in (2.4).

The Cayley graph (where elements of the groups are nodes and there is a link between two vertices if there exists a group multiplication taking one to another) for Γ is a freely generate trivalent tree, with each trivalent vertex replaced by a triangle. The triangles correspond to $S^3 = I$ and the edges, to $T^2 = I$. For any finite index subgroup Γ' of Γ we can let vertices be cosets of Γ' within Γ and likewise create a graph, this time finite (number of vertices is equal to the index, the number of cosets). This is the Schreier-Cayley coset graph for Γ' and is a finite trivalent graph. In fact, every finite trivalent graph can be generated this way: one could find some appropriate $\Gamma' \subset \Gamma$. The point is that all Schreier-Cayley coset graphs are *clean dessins*, by placing a black node on every edge. For instance, our running example⁵ of figure 1 is the coset graph for the congruence subgroup $\Gamma(4)$.

In [35], all torsion-free, genus zero⁶, congruence subgroups were classified. There are only 33 of them. The conjugacy class decomposition of the modular group using these subgroups leads to indexes: $\{6, 12, 24, 36, 48, 60\}$, where the restriction to a multiple of 6 is shown through use of the Riemann-Hurwitz formula (see [14] for a detailed review).

⁴More technically, a principle congruence subgroup is the kernel of a reduction modulo n morphism, i.e., it is what maps to the identity under $\pi_n : SL(2, \mathbb{Z}) \rightarrow SL(2, \mathbb{Z}/n\mathbb{Z})$. A congruence subgroup is then any subgroup which contains a principle congruence subgroup for some $n \geq 1$; additionally the smallest n such that the n th principle congruence subgroup is contained is known as the level of the subgroup [41].

⁵There is a peculiar ADE story here, the coset graphs for $\Gamma(m)$, $m = 3, 4, 5$, are precisely the tetrahedron, the cube/octahedron and the dodecahedron/icosahedron.

⁶The genus here means the genus of modular curve formed from the quotient of the subgroup's action on the upper half plane \mathcal{H} . Genus zero means that \mathcal{H} quotiented by the subgroup is simply a Riemann sphere.

The action of the modular subgroups can be extended from \mathcal{H} to $\mathcal{H} \times \mathbb{C}$ such that:

$$(\tau, z) \mapsto \left(\gamma\tau, \frac{z + m\tau + n}{c\tau + d} \right), \quad \text{for } \gamma = \begin{pmatrix} a & b \\ c & d \end{pmatrix}, \quad m, n \in \mathbb{Z}, \quad (2.5)$$

where γ denotes action of an element of one of the subgroups. Now taking the quotient of $\mathcal{H} \times \mathbb{C}$ by this extended automorphism gives the modular curve from before the extension with an elliptic fibration to form the unique 'modular surface' for that subgroup, called the Shioda surface. The index of the subgroup used gives the Euler number of the corresponding modular surface [14].

The modular surfaces formed from the index 24 torsion-free genus zero congruence subgroups are K3 surfaces, whilst those from index 36 subgroups are Calabi-Yau 3-folds (although these are instead fibrations over $\mathbb{P}^2_{\mathbb{C}}$) [14]. As an aside, from here dessins may also be considered to nicely arise as the structure of brane tilings formed from these Calabi-Yau manifolds when used in Type IIB superstring theory [24]. The point is that whilst only 9 of the 33 torsion-free congruence subgroups are index 24 and give K3 surfaces, it was realized in [14] that if you relax the condition that the subgroup has to be defined by some congruence (mod) relation, then you can obtain all extremal K3 surfaces, to which we now turn.

2.2.2 Dessins from j -maps

Now, a surface elliptically fibred over \mathbb{P}^1 takes the form of a Weierstraß equation:

$$y^2 = x^3 + g_2(z)x + g_3(z), \quad (2.6)$$

where the coefficients g_2 and g_3 are functions of the base Riemann sphere's complex coordinate z . The modular discriminant is

$$\Delta := 4g_2(z)^3 - 27g_3(z)^2, \quad (2.7)$$

and as a discriminant it indicates the degeneracy of roots of the cubic part of the Weierstraß equation. Modular forms are particularly useful in creating Galois representations, as well as appearing in many other useful areas of mathematics also. In general they are holomorphic functions on \mathcal{H} , and satisfy the condition

$$f\left(\frac{az + b}{cz + d}\right) = (cz + d)^k f(z), \quad (2.8)$$

for weight k . This condition shows the response of a modular form to action of the modular group on its input. Using the modular discriminant, a weight zero modular form can be defined, this is known as the **j-invariant**:

$$j(z) := \frac{4g_2(z)^3}{\Delta} = \left(\frac{4g_2(z)^3}{4g_2(z)^3 - 27g_3(z)^2} \right), \quad (2.9)$$

which is a modular function (in fact the unique one that generates the field of modular-invariants). Since the form is weight zero it is hence invariant under action of the modular

group. These j -invariants can therefore be considered as endomorphisms of the Riemann sphere, which are ramified at $\{0, 1, \infty\}$. Note that some definitions of $j(z)$ may include an additional factor of 1728, requiring a further Möbius transformations to convert the second ramified point from $1728 \mapsto 1$ [36].

The key observation is that due to the ramification structure of (2.9), the j -invariant, is Belyi! For $j(z) = 0$ this requires $g_2(z) = 0$, and the cubic dependence on it in the invariant function makes each root into a three-fold ramification point; these are the white nodes of the dessin. Equivalently $j(z) = 1$ requires $g_3(z) = 0$, and the square dependence here makes each root into a two-fold ramification point; the black nodes. Finally the $j(z) = \infty$ singularities require the modular discriminant $\Delta = 0$ (or $z \mapsto \infty$). Thus, each modular surface gives a dessin via its j -invariant.

In particular, the degree of the j -invariant's numerator equals the surface's index (here 24). So that the $z \mapsto \infty$ limit remains a singularity we require the denominator to have a lower leading order, hence the g_2^3 and g_3^2 factors but be of the same degree (both being 24), so the leading power of g_2^3 can be negated. This makes the invariants g_2 and g_3 of degree 8 and 12 respectively, leading to 8 trivalent white nodes, and 12 bivalent black nodes in these dessins.

Henceforth, we will focus on **extremal K3 surfaces** where all singular fibres are of Kodaira type I_n and there are exactly 6 of these fibres (q.v. [33] and [14] for further discussions). These 6 Kodaira singularities act as a 6-part partition of the mapping's degree (which is 24), giving the passport information. These 6 ramifications induce the 6 faces of the dessins (including the outside face, since the dessin is truly drawn on a sphere). There are 112 elliptic modular K3 surfaces which are extremal (indeed, there are 199 6-partitions of 24 but [33] showed only 112 are allowed) and we will focus on these in this paper. Note that if dessins are in the same Galois orbit they necessarily have the same passport (but not vice versa).

For instance, our example in figure 1 corresponds to

$$\begin{aligned} g_2(z) &= \frac{1}{\sqrt[3]{4}}(z^8 - 14z^4 + 1), \\ g_3(z) &= \frac{1}{3\sqrt{3}}(z^{12} + 33z^8 - 33z^4 - 1). \end{aligned} \tag{2.10}$$

Using these functions in (2.6), the Weierstraß equation for the modular surface is:

$$y^2 = x^3 + \frac{x}{\sqrt[3]{4}}(z^8 - 14z^4 + 1) + \frac{1}{3\sqrt{3}}(z^{12} + 33z^8 - 33z^4 - 1), \tag{2.11}$$

which then gives the defining equation of the K3 surface as a hypersurface in the anticanonical bundle of $\mathbb{P}_{[x:y:z]}^2$ via the Weierstrass equation (2.6). This is the modular surface which corresponds to the extended quotient action of the congruence modular subgroup $\Gamma(4)$ on \mathcal{H} .

2.3 The Dessin Database

In summary, we study 112 extremal semi-stable K3 elliptic fibrations, in which case the modular K3 surfaces have index 24. The j -invariant of each is a Belyi map with passport

$$\left\{ \begin{array}{c} 3^W \\ 2^B \\ n_1^{a_1}, n_2^{a_2}, \dots, n_k^{a_k} \end{array} \right\}, \quad \begin{array}{lll} W & = & \text{number of preimages of 0} \\ B & = & \text{number of preimages of 1} \\ \{n_i^{a_i}\} & = & \text{cusp widths of elliptic modular K3 surface} \end{array} \quad (2.12)$$

such that

$$\sum_i a_i = 6, \quad \sum_i a_i \cdot n_i = 24. \quad (2.13)$$

Each dessin is planar, trivalent, and clean and corresponds to a Schreier-Cayley coset graph of a particular subgroup of the modular group $PSL(2; \mathbb{Z})$. Of these, 9 are congruence subgroups, including the principal ones $\Gamma(m)$, $m = 3, 4, 5$.

All such K3 surfaces and associated dessins were classified in [33] and [34], the cartographic and modular subgroups were computed in [14]. The reader is also referred to the website [38] for the hand-drawn dessins. For reference, we include all dessins (along with their field extensions and adjacency matrices) in appendix C. Of these surfaces only 9 correspond to congruence subgroups, the remainder correspond to more general subgroups [14, 33].

One might note that there are more than 112 diagrams and there are, in fact, 191 dessins in the dataset. There are 112 distinct passports in this dataset, however the dessins sort themselves into 125 orbits of varying degree extension, where the degree of extension is equal to the size of the orbit. In some cases, for example 8-8-3-3-1-1 in appendix C, there are multiple orbits per passport (here one orbit of size one - with no degree extension, and one orbit of size two - with quadratic degree extension); and this accounts for the extra 13 orbits.

Within orbits some graphs are isomorphic, this is where some roots of the minimal polynomial are complex. Since the minimal polynomial is defined over the field of (real) rational numbers, any root with non-zero imaginary part also has its complex conjugate as a root. These pairs of conjugate roots of the polynomial correspond to dessins which are isomorphic, but chirality flipped. For example in appendix C, considering passport: 7-6-5-3-2-1, there is one orbit associated to this passport which is cubic, it hence has 3 dessins belonging to it, corresponding to the 3 roots of a cubic polynomial (the minimal polynomial). As the polynomial has only real rational coefficients, its roots must be decomposed into: one real root, and one pair of complex conjugate roots (note there could have been 3 distinct real roots, but here this is not the case). The conjugate pair gives the isomorphic B & C dessins, which share the same adjacency matrix. Therefore there are only 155 distinct matrices in the dataset, corresponding to the 155 dessins unique up to isomorphism. To further exemplify this, note that in some cases (7-7-3-3-2-2) the polynomial has distinct real roots giving non-isomorphic dessins, but in others (7-7-4-4-1-1) the roots are a complex conjugate pair giving isomorphic dessins, but flipped. As explained in §2.1.2, dessins are embedded graphs so how they are drawn on the Riemann sphere makes a difference.

Because our dessins are clean, it suffices to only draw the white nodes and the graph is, at least combinatorically, completely captured by 8×8 **adjacency matrices** which we will define shortly. These are shown next to the dessins in the appendix, and will constitute the data input to be analysed in §3.

As mentioned, one key feature of a dessin d'enfant is the algebraic field in which the algebraic model for the underlying Riemann surface X (as well as the Belyi map) lives. Oftentimes, the minimal polynomial defining the extension, even for relatively innocuous looking dessins, could be enormous and because dessins are number-theoretic, the coefficients in these polynomials are completely rigid and are very precise integers (giving the roots as specific algebraic numbers). For example, for the relatively simple brane-tiling of the so-called $X^{3,0}$ toric gauge theory, the defining polynomial's coefficients were found [42] to be integers on the order of 10^{200} .

Importantly, for our dataset, the Weierstraß equation of the K3 surface is defined over \mathbb{Q} , or some extension of \mathbb{Q} involving a square, cubic, or quartic root. This means that the extension degree of all our dessins are 1, 2, 3, or 4 (where 1 means \mathbb{Q} itself). Where the field is an extension of \mathbb{Q} , the Galois representation maps between the roots of the polynomial defining the extension and in each case this corresponds to a different dessin. Hence the number of dessins corresponding to each passport equals the sum over the orbits' field extension degrees for all orbits with this passport ramification data. For example, in appendix C, passport: 10-10-1-1-1-1, has 3 dessins; it also has two orbits (one degree 2 from the quadratic extension, and one degree 1 where there is no extension), satisfying the $3 = 2 + 1$.

2.4 Seiberg-Witten Theory

In this final subsection of setting the stage, we come to the physics of our dessins.

2.4.1 Sieberg-Witten Curves

Sieberg-Witten theory [9] considers the low energy IR limit of $\mathcal{N} = 2$ supersymmetric gauge theories. More specifically it allows for exact description of the coulomb branch vacuum manifold by defining it in terms of a hyperelliptic curve - the 'Sieberg-Witten curve'. Now, points of the $\mathcal{N} = 2$ vacuum manifold defined by the hyperelliptic curve can be lifted to $\mathcal{N} = 1$ vacua through deformation with a tree level superpotential. At these special points, which are singularities of the manifold, dessins naturally arise as combinatoric representations of the root structure of the Sieberg-Witten hyperelliptic curve. A correspondence can hence be considered between phases of the $\mathcal{N} = 1$ vacua and classes of dessins in Galois orbits [8].

For a general $U(N)$ gauge theory with L massive scalars (masses m_i respectively), the Sieberg-Witten curve takes the form:

$$y^2 = \langle \det(zI - \Phi) \rangle^2 - 4\Lambda^{2N-L} \prod_{i=1}^L (z + m_i), \quad (2.14)$$

with Φ the adjoint scalar in the coulomb branches vector multiplet, Λ , a cut-off measure which controls the energy limit of the theory [8, 43], and the deformation term (second on the RHS) is prescribed by the $\mathcal{N} = 1$ superpotential.

The insight of [8] is that (2.14) can be identified with Belyi maps of clean dessins by first making the association:

$$\begin{aligned} P_N(z) &:= \langle \det(zI - \Phi) \rangle, \\ B(z) &:= -4\Lambda^{2N-L} \prod_{i=1}^L (z - m_i). \end{aligned} \quad (2.15)$$

In addition another function $A(z)$ is defined, such that it has an equivalent form to the function $B(z)$, which can more generally be written

$$A(z) = \prod_i J_{u_i}^i(z), \quad B(z) = \prod_i G_{v_i}^i(z), \quad (2.16)$$

for J_{u_i} and G_{v_i} as sets of polynomials of degrees u_i and v_i respectively. These functions are designed so as to satisfy the relation: $A - B = P_N^2$. Then, the map defined by

$$\beta(z) := \frac{A(z)}{B(z)} = 1 + \frac{P_N^2(z)}{B(z)}, \quad (2.17)$$

is Belyi. The preimages of 0 correspond to the roots of $A(z)$, due to the form of $A(z)$ defined in (2.16) each of the J_{u_i} polynomials of degree u_i will lead to u_i roots, and as the whole polynomial is raised to the power of i in $A(z)$'s definition, each root/ramification point will have valency i also. Correspondingly the roots of $P_N(z)$ give the Belyi map preimages of 1, and since it is squared in the Belyi map definition these points will have valency 2 - giving clean dessins exclusively. Finally the preimages of ∞ , the final ramification point of the Belyi map, are given by the roots of $B(z)$ (as well as the $A(z) \mapsto \infty$ limit).

A general Seiberg-Witten (SW) curve does not factorise as simply as represented by (2.16). However tuning the superpotential parameters can cause the roots of the functions to coincide, giving this polynomials raised to powers structure. It is at these isolated singularities along the $\mathcal{N} = 1$ branches caused by the superpotential tuning that the dessins are formed from the usual branch-less structure of the roots, since the roots now have higher valencies.

Specifically, for the dessins we are considering, $A(z)$ and $B(z)$ take the form:

$$A(z) = J_8^3, \quad B(z) = G_{12}^2, \quad (2.18)$$

to match the form of the passport given in §2.1.1.

In the physical theory at these points the superpotential has triggered a magnetic Higgs mechanism. Here the symmetry breaking of the full gauge group for the $\mathcal{N} = 2$ Seiberg-Witten curve leaves a residual symmetry group preserving a submanifold of the curve which corresponds to one of the $\mathcal{N} = 1$ vacua. Thus, there are number-theoretic special points in $\mathcal{N} = 1$ vacua. Indeed, [15] further associates elliptic K3 surfaces and modular congruence subgroups to these distinguished points.

A primary aim in the field of Galois theory is to find invariants which can distinguish between different orbits of $Gal(\overline{\mathbb{Q}}/\mathbb{Q})$. Since these orbits correspond to orbits of dessins, they thus also provide tools for distinguishing between different branches of the $\mathcal{N} = 1$ vacua. The tools they relate to are holonomy measures for the gauge connections of the residual symmetry groups occurring at these $\mathcal{N} = 1$ vacua. Through this connection if there is an exact correspondence between all invariants distinguishing Galois orbits, and order parameters which distinguish vacua branches, there is potential to draw physical insight from the use of dessins more explicitly in the physical theories [8, 44].

2.4.2 Dessins to Seiberg-Witten Curves

Thus armed, we can now put our foregoing discussions together and algorithmically follow the process laid out in Cachazo et al. [8] to convert the Belyi maps of the relevant dessins, some of whose Belyi maps have already been computed by F. Beukers [38], into Seiberg-Witten curves.

We reverse the procedure in (2.16) and (2.17), and for convenience set $\alpha := -4\Lambda^{2N-L}$. Then starting with (2.17), where $A(z)$ and $P_N(z)$ are monic polynomials and $B(z) = \alpha \prod_i^L (z - m_i)$ with m_i as the complex roots of $B(z)$. The SW curve is then given by:

$$y^2 = P_N(z)^2 + \alpha \prod_i^L (z + m_i). \quad (2.19)$$

The polynomials for the Belyi maps of dessins with rational coefficients are provided in reference [38] with the following correspondence to the polynomials listed above:

$$\begin{aligned} A(z) &= x^3(z)/a, \\ B(z) &= k(z)/a, \\ P_N^2(z) &= y^2(z)/a, \end{aligned} \quad (2.20)$$

where a is a constant that may be required to make the polynomials $A(z)$ and $P_N(z)$ monic. The algorithm for this computation is given by Algorithm 1.

Algorithm 1: Algorithm taking Belyi maps and calculating the equivalent SW curve

Input: $x(z)$ and $k(z)$
Output: y^2 , the SW curve corresponding to the Belyi map $\frac{x^3}{k}$

$$q(z) = x^3(z) - k(z)$$

 a = coefficient in front of the highest order term in $q(z)$

$$P_N^2(z) = \frac{q(z)}{a} \text{ // Now } P_N \text{ is a monic polynomial}$$

$$B(z) = \frac{k(z)}{a} \text{ // Now the polynomials are in the form required by the correspondence above}$$

 α = coefficient in front of the highest order term in $B(z)$

$$B'(z) = \frac{B(-z)}{\alpha}$$

 $B'(z) = \pm B'(z) \text{ // Needed to keep the leading order term positive}$

$$y^2 = P_N^2(z) + \alpha \cdot B'(z)$$

For our running example of figure 1, we make use of (2.3) and (2.14) and substitute the relation: $P_N^2(z) = A(z) - B(z)$. Then noticing that since the roots of $B(z)$ (given by the preimages of ∞ in table 1, excluding ∞) are either 0 or occur in \pm pairs, then the form swap

$$B(z) = \alpha \prod_{i=1}^L (z - m_i) \longmapsto \alpha \prod_{i=1}^L (z + m_i) = B(z), \quad (2.21)$$

reproduces $B(z)$. This makes the Seiberg-Witten curve

$$y^2 = (A(z) - B(z)) + B(z) = A(z) = (z^8 - 14^4 + 1)^3, \quad (2.22)$$

as given in appendix B.

Now, when the field extension is degree 1 (i.e., all coefficients in β are rationals and scalable to integers), the Belyi maps have been computed by [38]. We start from these and obtain the list of SW curves, as presented in appendix B.

3 Classifying the Dessin Extensions

We now come to the highlight of our computations, where a simple fully connected Neural Network (NN), with no knowledge of the underlying mathematics, was created that is able to predict the extension degree.

3.1 Data Engineering

We begin by setting up the data. Because the dessins are all clean, the information from the black nodes can be suppressed (each edge has one, and only one black node) and we only

need to know how the white nodes are linked (in fact, each white node has valency 3 by construction). Thus, graph-theoretically, each dessin is captured by adjacency matrices \mathcal{M} , defined such that:

- Each vertex for a given dessin is labelled between 1 and 8.
- If a single edge connected vertices i and j then a 1 was entered in the element \mathcal{M}_{ij} and \mathcal{M}_{ji} .
- If there were 2 edges connecting these vertices then a 2 would be entered into the corresponding element. If an edge connected a vertex to itself then this would count as 2 connections and hence a 2 was entered as that element \mathcal{M}_{ii} , etc.

As the dessins are not directed, the adjacency matrices are symmetric. The dessin dataset, along with the corresponding matrices are shown in appendix C.

We make a few remarks. First, \mathcal{M} is defined only up to permutation via relabelling the nodes, so we need to take this into account. Next, we see from the appendix that multiple dessins could have the same \mathcal{M} . Luckily, these are precisely Galois conjugates so they have the same extension degree. Therefore, there is no ambiguity in our classification problem.

As is well established, the effectiveness of a NN is almost always improved by increasing the size of the dataset used to train it [45, 46]. To artificially increase the size of the dataset from just shy of 200 to 160,000 we precisely exploit the freedom in choice of relabelling the vertices. Algorithm 2 loops through every unique pair of vertices a, b and outputs the adjacency matrix that would have been created, by following the rules above, if vertex a was labelled as b and vertex b labelled as a . This algorithm was applied twice, firstly to the matrices constructed directly from the dessins and then to that output, each time increase the amount of data by a factor of 29.

The proportion of the dataset that had a particular extension was as follows: rational 39.8%, quadratic 34.6%, cubic 23.6%, quartic 0.02%. These were the same before and after the data extension.

In summary, we now have a labelled dataset of size around 160,000 of the form

$$\mathcal{M}_{8 \times 8} \longrightarrow \text{Extension Degree over } \mathbb{Q} , \quad (3.1)$$

where the degree is 1, 2, 3 or 4. This constitutes a perfect 4-category classification problem for machine-learning.

Algorithm 2: Algorithm to increase the size of the dataset. It loops through all pairs of vertices and creates a new adjacency matrix as if these 2 vertices were labelled as each other.

Input: \mathcal{M} , The original adjacency matrix of the dessin

Output: \mathcal{M}' , The new adjacency matrix after vertices have been relabelled. Outputs a new matrix for every (a, b) combination

for $a = 1$ **to** 7 **do:**

for $b = a + 1$ **to** 8 **do:**

 // a and b are the indices in \mathcal{M} of the vertices performing the label swapping

for $i = 1$ **to** 8 **do:**

 // i and j are the indices of the new element of \mathcal{M}'

if $i \neq (a \text{ or } b)$ and $j \neq (a \text{ or } b)$ **then:**

$\mathcal{M}'_{ij} = \mathcal{M}_{ij}$

else if $i \neq (a \text{ or } b)$ and $j = b$ **then:**

$\mathcal{M}'_{ib} = \mathcal{M}_{ia}$

 :

 and so on for all combinations of i and j . If an element of \mathcal{M}' has an index of ' a ' then the value of that element is equal to the corresponding element of \mathcal{M} where the relevant index is replaced by ' b ' and vice versa

 :

output: save the current \mathcal{M}'

3.2 Setup of the Machine-Learning Model

We create a deep feed-forward neural network (a multi-layer perceptron) using the TensorFlow Keras Library [47], consisting of several fully connected (known as dense in the Keras documentation) layers [48, 49]. The activation function for each of these fully connected layers was the ReLU function⁷. Finally, the output layer was a dense layer with 4 neurons with the softmax activation function⁸. The output of each of these 4 neurons represents the probability that the dessin had a particular extension. A schematic of this model is found in figure 2.

⁷This is the Re(ctified) L(inear) U(nit), defined as $f(x) = \max(0, x)$ for $x \in \mathbb{R}$.

⁸A soft max layer returns n floating point values which sum to unity. Each value represents the probability that input is of a particular category. That is, $f(z_i) = \exp(z_i) \left(\sum_{j=1}^k \exp(z_j) \right)^{-1} : \mathbb{R}^k \rightarrow \mathbb{R}^k$.

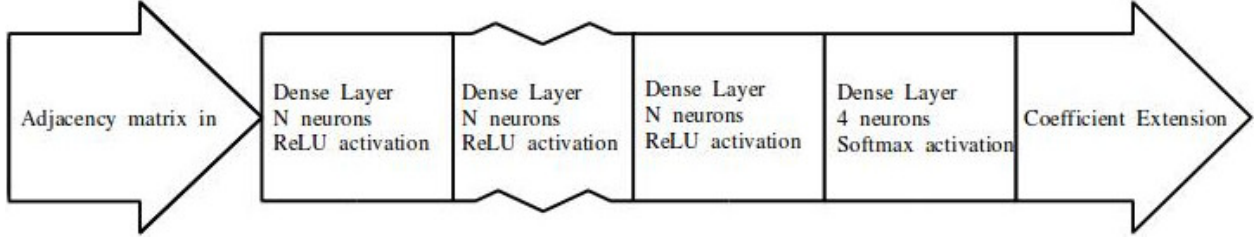


Figure 2: Schematic showing the details of the neural network. All of the layers, excluding the output layer, have the same hyper-parameters.

The model was complied with the following specifications [47]:

- Loss function: `sparse_categorical_crossentropy`. When training the model, the parameters of the NN get adjusted to minimise the loss function. Cross-entropy is the required loss function for discrete categories of data [49]. Specifically, the cross-entropy used is $-\frac{1}{n} \sum_{j=1}^n \sum_{i=1}^C y_i^j \log(\hat{y}_i^j)$ where n is the number of samples in the training, indexed by j and C is the number of categories (here 4), indexed by i . Moreover, y is the sample label (here the extension degree) and \hat{y} is the predicted value for the degree.
- Optimizer: `adam` with the default Keras hyper-parameters. Adam is one of the many modern improvements on the stochastic gradient descent algorithm. Comparison with other, similar, optimizers suggest `adam` to be the best generic choice [50].
- Metric: `accuracy`. Metrics do not influence the training of the model, they specify what data to output at the end to judge the effectiveness of the model. `accuracy` means the output is the fraction of predictions the model got correct [47].

To measure the bias we introduce a bias loss function defined as:

$$L = \left(\sum_i \left(\frac{\frac{\tilde{n}_i}{N_{\text{test}}} - \frac{n_i}{N_{\text{total}}}}{\frac{n_i}{N_{\text{total}}}} \right)^2 \right) / N_i, \quad (3.2)$$

the summation is over all the different categories, $\tilde{n}_i/N_{\text{test}}$ is the predicted fraction of that category in the test (/validation) data, n_i/N_{total} is the actual fraction of that category in the training data (as the training data is much larger than the test data it doesn't matter if this is the fraction of that category in just the training data or in the both test and training data combined), and N_i is the number of categories. This measure gives the average fractional difference between the predicted and actual fraction of each category.

3.3 NN Results

The style of machine-learning used in this study is: *supervised* learning. In this style the initial dataset is partitioned into a training set and a test set; and both sets are composed of

Parameters	Accuracy	MCC					Bias Loss Function
		Q	Square	Cubic	Quartic	Multiclass	
Epochs: 31							
Layers: 5	0.930	0.87	0.86	0.91	0.91	0.88	0.21
Neurons: 256							
Epochs: 17							
Layers: 5	0.935	0.89	0.87	0.91	0.75	0.88	0.23
Neurons: 512							
Epochs: 31							
Layers: 4	0.939	0.88	0.85	0.90	0.84	0.87	0.22
Neurons: 512							

Table 2: The results of three neural networks in predicting degree of extension of elliptically fibred K3 surfaces. Results show the accuracy and MCC measures, as well as the bias loss function for each network.

defined inputs (here adjacency matrices) and outputs (here degrees of the field extension). The network is fed the training set, as many times as the number of epochs specified, during the fitting process. Then after the network has been trained, it is tested (or 'evaluated') on the test data which it has not seen before. The proportion of correct classifications on the unseen test data gives the accuracy measure of the network's success.

The other measure is Matthew's Correlation Coefficient (MCC), it is defined in reference to the confusion matrix which is a 4-entry matrix measuring probabilities of correct (positive) and incorrect (negative) predictions of True and False hypotheses respectively. Using this, MCC is defined as the square root of the normalised χ^2 statistical measure:

$$\phi := \sqrt{\frac{\chi^2}{N}} = \frac{tp \cdot tn - fp \cdot fn}{\sqrt{(tp + fp)(tp + fn)(tn + fp)(tn + fn)}}, \quad (3.3)$$

for $\{tp, tn, fp, fn\}$ representing $\{\text{true positive, true negative, false positive, false negative}\}$ respectively [22].

From the dataset 300 dessins were selected, at random, to act as the test data, and the rest were used to train the model. A different random set was selected every time the NN was trained and tested, removing systematic errors that could have occurred if the test data was not representative of the whole population.

Once the general model was setup a range of different parameter choices were tested, with each choice being trained and tested 5 times, and averages taken. Compiling and testing the models took on the order of about an hour each using a standard personal computer (64 bit, i5 2.7Ghz i5 dual core, 16GB ram, linux mint). Combinations of the following parameters were tried:

- Epochs: 10, 17, 24, 31. This is the number of times the NN runs through the dataset.
- Layers: 3, 4, 5. Each layer was the same type (dense), had the same number of neurons

and same activation function (ReLU). Note that this number does not include the final output layer which was a dense softmax layer with 4 neurons.

- Neurons per layer: 64, 128, 256, 512.

Table 2 shows, for all setups that resulted in over 93% accuracy, the parameters, Matthews Correlation Coefficient (MCC) [51] and the evaluation of the Bias Loss Function. The individual correlation coefficients given were calculated as if they were binary data: a result was considered positive if the network’s prediction gave the correct degree, and negative if it was predicted to be any of the other three degrees. For the total correlation coefficient the multi-class case was used as given in the reference above.

The final figure, figure 3, shows the learning curves monitoring the NN’s accuracy over the training epochs. The NN quickly reaches high accuracies of classification in few epochs, and with large amounts of data held back from validation such that less data is used in training the NN.

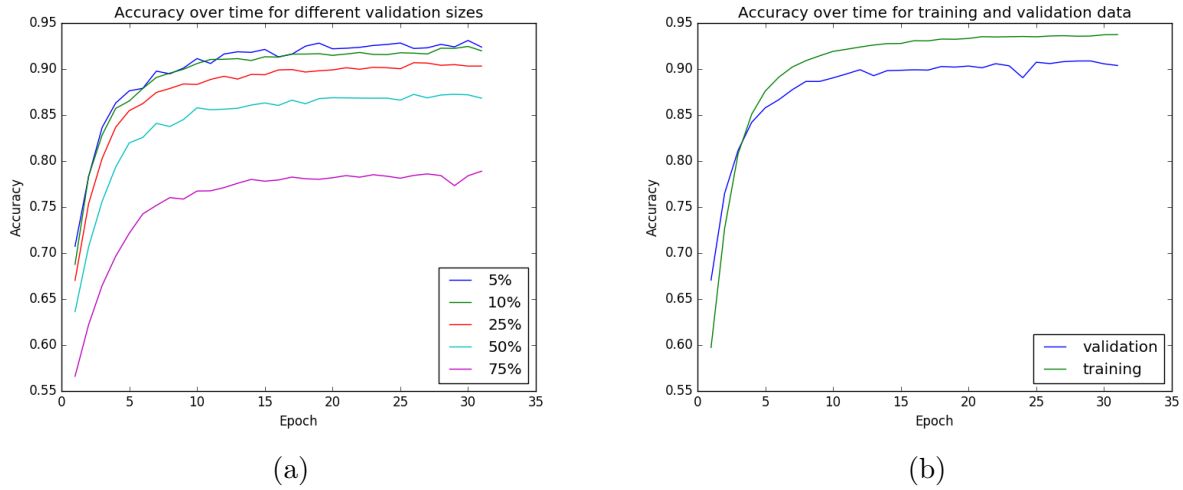


Figure 3: (a) shows how varying the proportion of the data held back for validation affects the overall accuracy of the model. The model quickly converges to an above 0.85 accuracy for as little as 50% of the data used for training (s.t. 50% held back for validation). (b) compares the accuracy of the model when evaluated on the training data and when evaluated on the validation data, both showing consistently high accuracies for few epochs. Both figures are for the 4 layers, 512 neurons, 31 epoch model.

4 Conclusion & Outlook

In this paper we have initiated the study of machine-learning applied to dessins d’enfant, as part of the recently advocated programme to see whether AI can deep-learn structures of mathematics [18, 25, 22]. The key aspect of the programme is the following: given the rapid increase of available data in pure mathematics and mathematical physics, gathered over the last decade or so, ranging from algebraic geometry, to group theory and combinatorics, to number theory, can neural networks and classifiers - often without any prior knowledge of the underlying mathematics - uncover more efficient methods of computation and raise unexpected conjectures. As mentioned in the introduction, various experiments by a host of collaborations have shown this to be a fruitful venture.

As a concrete play-ground, we have taken 191 dessins which reside at the cusp of several intertwining fields of investigation: subgroups of the modular group, extremal elliptic K3 surfaces as Shioda modular surfaces, and $\mathcal{N} = 1$ Seiberg-Witten curves. We have first completed the mapping amongst these quantities in the present context. Then, we have launched the examination of the question: *can one “look” at a dessin and classify its degree of extension over \mathbb{Q} ?* Indeed, a central theme of Grothendieck’s *Esquisse* is to understand how dessins furnish a representation of the absolute Galois group which governs all algebraic extensions over \mathbb{Q} .

Rather surprisingly, we find that a simple multi-layer perceptron with standard activation functions such as ReLU and linear layers can classify this problem within our dataset, enhanced by permutation equivalence to a size of the order 10^5 , to over 90% accuracy and confidence around 0.9. This is quite contrary to the fact how difficult it is to compute explicit Belyi maps and to the intuition built over the last couple of years how number-theoretical problems respond poorly to machine-learning. Perhaps, dessins are closer to complex analysis than to number theory, as opposed to BSD [32], which seems more resilient to modern data-scientific methods.

Of course, we have only skimmed the surface. There is an infinitude of dessins of varying complexity and it is known that $Gal(\overline{\mathbb{Q}}/\mathbb{Q})$ acts even faithfully on genus 0 and genus 1 families thereof individually. Can our neural network extrapolate to these? Indeed, as a part of more ambitious plan, can we establish machine-learning models which help compute actual Belyi maps? Indeed, what about other aspects of dessins, such as cartographic groups and permutation triples, many of which have also found their place in theoretical physics; can these be machine-learnt? There are undoubtedly many other questions we leave to future investigations.

Acknowledgements

YHH would like to thank STFC for grant ST/J00037X/1. EH would like to thank STFC for the PhD studentship.

Appendix A Reproducing the Riemann Surface

To further motivate the study of dessins, importantly one can reproduce the Riemann surface's algebraic curve, X , used in the Belyi pair definition of a dessin, as described in §2.1.1, up to a homeomorphism. In this process the dessin is triangulated, and this triangulation also proves important in linking the dessins to the finite set category.

Starting with a dessin, first vertices are introduced into each isolated part of the dessin (i.e., one within each loop, and another outside the dessin); these are associated to the points of the Belyi function ramified at infinity. Then edges from each of these 'infinity' vertices are drawn to all vertices of the dessin along the boundary of the isolated section of the dessin. This is all vertices which edges can be drawn to without having to cross another edge, noting there may be duplicate vertices where the vertices appear more than once in the region's boundary.

This process triangulates the dessin, such that all the isolated sections are now bound by 3 vertices (one of each of $\{\text{white } \circ, \text{ black } \bullet, \text{ infinity } \infty\}$). This is shown in figure 4. If the triangle is bounded in a clockwise/anticlockwise direction by the vertex order: white \mapsto black $\mapsto \infty$; then the section is associated to a lower/upper half plane. The half planes are then glued along the appropriate boundaries [4]. Importantly since the dessin is truly embedded on the Riemann sphere in our case, the outside 'face' is identified with the opposite half plane to the usual vertex ordering of the boundary as seen from the representation in the figure.

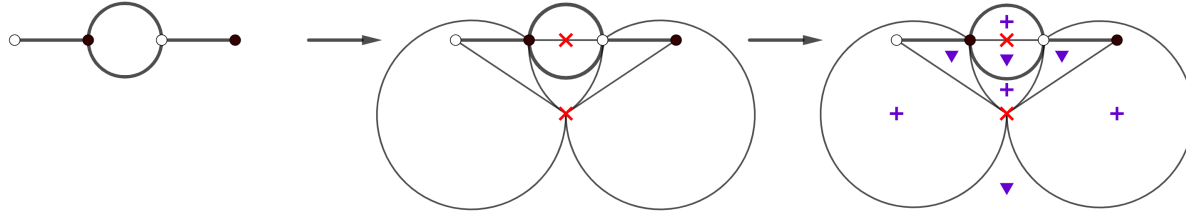


Figure 4: The process of converting a dessin into the corresponding Riemann surface. The first graph shows an arbitrary dessin. The second shows the inclusion of the 'infinity' ramification vertices (red crosses) in each isolated region of the dessin; and the additional edges drawn to all vertices bounding the region - the triangulation process. The final graph shows each triangulated region associated to either the lower (blue triangle) or upper (blue plus) half planes according to the boundary orientations. These planes are then glued together along each boundary to give the Riemann surface.

This produces a Riemann surface homeomorphic to the original X in the Belyi pair used to define the dessin. Note since the graph-theoretic degree of a vertex leads to twice as many half planes around it, which are correspondingly glued, it becomes clear this degree represents the ramification degree of the surface cover. This Riemann surface produced may then be mapped to the Riemann sphere, and this mapping is then equivalent to the Belyi function from the original Belyi pair, up to a biholomorphism. Therefore an equivalent Belyi pair is produced, and the relation between these pairs is appropriately defined within the Galois-theoretic structure.

After triangulation there now exists three order 2 permutations on the triangles, which are reflections in each of the triangles edges. The full cartographic group is then the group of permutations of these triangles generated by these 3 reflections. Combining the reflection operators (denoted a , b , and c), three permutation operators can be defined: $\{\sigma, \alpha, \phi\} := \{ab, bc, ca\}$ respectively; note that also due to the order two nilpotence of reflection operators

$$\sigma \cdot \alpha \cdot \phi = 1. \quad (\text{A.1})$$

Since each triangle is associated to one edge from the original dessin, these permutation operators may be thought of as generating permutations of the dessin. This defines the cartographic group, as the edge set permutations generated by these permutation operators. However due to the property from (A.1), only two generators are required. This then defines the equivalence, there is a bijection between isomorphism classes of dessins (under permutation) and conjugacy classes of finite index subgroups of the free group generated by $\{\sigma, \alpha\}$. This gives another practical use for dessins in examining free groups [5].

Appendix B Generated Seiberg-Witten Curves

Here we include the Seiberg-Witten curves for all dessins with rational coefficients, and hence defined over the field \mathbb{Q} , as listed in appendix C, and [34]. Note those defined over fields which are extensions of the rationals are not included.

Dessin	SW curve $y^2 =$
19, 1, 1, 1, 1, 1	$-\frac{135z^4}{2} - \frac{81z^2}{2} + (z^8 - 2z^7 + 7z^6 - 6z^5 + 11z^4 + 4z^3 + 12z + 1))^3 + \frac{837}{2}$
18, 2, 1, 1, 1, 1	$\frac{1}{729}((9z^8 + 36z^6 + 54z^4 + 28z^2 + 1))^3$ $\frac{1}{((9z^4 - 14z^3 - 9z^2 + 6z + 21))(4z + 1)^3 + (54z^{12} + 162z^{11} - 270z^9 + 162z^8 + 432z^7 - 252z^6 - 216z^5 + 270z^4 - 63z^2 + 21z - 5))^2}{2916}$
17, 3, 1, 1, 1, 1	$((z^8 + 16z^4 + 16))^3$
16, 4, 1, 1, 1, 1	$\frac{1}{729}((-165888z^7 - 442368z^3 + ((9z^8 + 48z^7 + 64z^6 + 48z^4 + 128z^3 + 16))^3))$ $(z^8 - 8z^6 + 20z^4 - 16z^2 + 1)^3$
16, 3, 2, 1, 1, 1	$\frac{1}{729}((-64(z - 1)^3(z^3 - 3z - 3)(3z - 4)^3 + 64(z + 1)^3(3z + 4)^3(z^3 - 3z + 3) +$ $(z^2 - z - 1)^3(9z^6 - 27z^5 + 45z^3 - 51z + 23)^3)$
15, 3, 1, 1, 1, 1	$-1728(z^2 - 3z + 1)^2(z^2 + 6z + 10)(2z - 5)^3 + 1728(2z + 5)^3(z^2 - 6z + 10)(z^2 + 3z + 1)^2 +$ $(z^2 - 5)^3(z^6 - 15z^4 + 75z^2 - 48z - 5)^3$
15, 3, 2, 2, 1, 1	$\frac{1}{207360z^9 + 912384z^7 + 387072z^5 + (25z^8 - 40z^7 + 56z^6 - 112z^5 + 32z + 16)^3}$
14, 4, 3, 1, 1, 1	$-8707129344(z - 5)^3(5z^3 - 3z^2 - 264z - 5980)(1 - 3z)^4 + 8707129344(z + 5)^3(3z + 1)^4(5z^3 + 3z^2 - 264z + 5980) +$ $(z^8 - 10z^7 - 35z^6 - 700z^5 + 10780z^4 - 12544z^3 + 12880z^2 - 677440z + 2843200)^3$
14, 3, 3, 2, 1, 1	$30233088z^9 - 120932352z^7 + 6348948480z^5 - 19863138816z^3 + (z^8 - 4z^7 - 14z^6 + 315z^4 - 1134z^2 - 1620z + 1377)^3 +$ $40814668800z$
14, 3, 3, 2, 1, 1	$-1259712(z + 8)^2(5z^2 + 21z - 441)(17z^2 - 71z + 59)^3 + 1259712(z - 8)^2(5z^2 - 21z - 441)(17z^2 + 71z + 59)^3 +$ $(z^8 + 12z^7 - 102z^6 - 1096z^5 + 4275z^4 + 22632z^3 - 90566z^2 + 42756z + 122913)^3$
14, 3, 2, 2, 2, 1	$\frac{1}{27(z - 4)(12z + 1)^2(3z^2 - 14z + 14)^2z^3 - 27(1 - 12z)^2(z + 4)(3z^2 + 14z + 14)^2z^3 + 4(9z^8 + 120z^7 + 616z^6 + 1512z^5 + 1764z^4 + 784z^3 - 12z + 1)^3}{2916}$
13, 7, 1, 1, 1, 1	$8460288z^{10} + 132865920z^8 + 135543240z^6 + \frac{26168373z^4}{290655z^2} + \frac{290655z^2}{26168373z^4} +$ $(z^8 + 6z^7 + 21z^6 + 98z^5 + 182z^4 + 210z^3 + 301z^2 - 214z + 4)^3 - \frac{135}{2}$
13, 5, 3, 1, 1, 1	$\frac{1}{729}(64(4z + 5)^3(5z^3 + 15z^2 - 9z - 355)(9z - 31)^5 - 64(4z - 5)^3(9z + 31)^5(5z^3 - 15z^2 - 9z + 355) +$ $(9z^8 - 180z^6 - 720z^5 + 2790z^4 + 7008z^3 - 7540z^2 - 38640z + 14825)^3)$
13, 4, 3, 2, 1, 1	$-918330048(109 - 5z)^2(8z - 73)^3(7z^2 + 730z + 21543)(303 - 17z)^4 +$ $918330048(5z + 109)^2(8z + 73)^3(17z + 303)^4(7z^2 - 730z + 21543) +$
13, 3, 3, 2, 2, 1	$(z^8 - 7z^7 - 1092z^6 + 135016z^5 + 1687350z^4 - 76683768z^3 - 1742916644z^2 - 9658896744z + 6717775617)^3$ $322486272(z + 10)(5z^2 - 24z + 612)^2(4z^2 - 17z + 430)^3 - 322486272(z - 10)(4z^2 + 17z + 430)^3(5z^2 + 24z + 612)^2 +$ $(z^8 + 240z^6 - 1600z^5 + 14880z^4 - 274944z^3 + 490240z^2 - 10544640z + 29606400)^3$
12, 6, 3, 1, 1, 1	$34012224(z - 3)^3(z^3 + 9z^2 - 216)(z - 4)^6 - 34012224(z + 3)^3(z + 4)^6(z^3 - 9z^2 + 216) +$ $(z^2 - 18)^3(z^6 - 54z^4 + 1620z^2 - 5184z + 4536)^3$
12, 6, 2, 2, 1, 1	$(z^8 + 8z^6 - 16z^2 + 16)^3$ $\frac{-13226976z^{11} + 56683704z^9 + 419904z^7 + (5184z^8 + 5184z^7 + 3024z^6 + 21z^2 - 6z + 1)^3}{1000000}$
12, 6, 2, 2, 2, 1	$\frac{139314069504}{z^5 + 432(14 - 5z)^2(z - 4)(70z^2 + 24z + 9)^2z^5 + 64(25z^8 + 240z^7 + 756z^6 + 784z^5 + 70z^2 - 24z + 9)^3}{1000000}$

$$\begin{aligned}
& \frac{108(7-4z)^4(z-2)^2(z^2+2)(z-1)^4-108(z+1)^4(z+2)^2(4z+7)^4(z^2+2)+(16z^8+128z^7+448z^6+960z^5+1488z^4+1728z^3+1392z^2+696z+177)^3}{4096} \\
& (z^8-12z^6+30z^4-12z^2+9)^3 \\
& 110592(z^2+12z+45)(5z^2-36z+65)^3(z-3)^4-110592(z+3)^4(z^2-12z+45)(5z^2+36z+65)^3+ \\
& (z^2-15)^3(z^6-45z^4+1155z^2-3456z+2865)^3 \\
& -1296z^{11}+6156z^9-11340z^7-8100z^5-216z^3+(z^8+8z^7+16z^6-8z^5-28z^4+16z^3+4z^2-4z+1)^3 \\
& 1728(z-4)^2(z+1)^3(z+5)(5z^2-8z-40)^3-1728(z-5)(z-1)^3(z+4)^2(5z^2+8z-40)^3+ \\
& (z^2-10)^3(z^6-30z^4+180z^2-192z-40)^3 \\
& (z^8+12z^6+48z^4+66z^2+9)^3 \\
& -\frac{27}{4}(z^4+14z^3+47z^2-102z+45)(4z-3)^9+\frac{27}{4}(4z+3)^9(z^4-14z^3+47z^2+102z+45)+ \\
& (z^8+18z^7+95z^6-18z^5-701z^4+1068z^3-432z^2-108z+81)^3 \\
& 1728(z^3+3z^2+11z+121)(4z^2-9z+91)^5-1728(4z^2+9z+91)^5(z^3-3z^2+11z-121)+ \\
& (z^8+44z^6-176z^5+374z^4-5984z^3+2156z^2-44176z+64801)^3 \\
& \frac{27}{4}(3z-53)(7z+43)^3(243-5z^2)^2(8z-141)^5-\frac{27}{4}(3z+53)(7z-43)^3(8z+141)^5(243-5z^2)^2+ \\
& (z^8-48z^7+588z^6+3304z^5-85470z^4-9408z^3+3745084z^2-923724z-45225702)^3 \\
& -1728(z-2)^3(3z^2+z+111)(5z^2-9z+9)^4+1728(z+2)^3(3z^2-z+111)(5z^2+9z+9)^4+ \\
& (z^8+6z^7+57z^6+278z^5+900z^4+2190z^3+3145z^2+1110z-855)^3 \\
& -1259712(z-26)^2(4z-153)(7z^2+4z+4)^3(9-5z)^4+1259712(z+26)^2(4z+153)(5z+9)^4(7z^2-4z+4)^3+ \\
& (z^8+96z^7+3192z^6+41888z^5+168000z^4+97440z^3+244720z^2-728640z-200880)^3 \\
& (z^8+12z^6+14z^4-12z^2+1)^3 \\
& \frac{1}{729}(-64(z+1)^3(11z^3-105z^2+1008z+124)(2-9z)^8+64(z-1)^3(9z+2)^8(11z^3+105z^2+1008z-124)+ \\
& (9z^8-108z^7+1062z^6-2196z^5+2385z^4+20568z^3+42104z^2+19104z+1808)^3 \\
& -442368(7z+15)^4(11z^3+3z^2-2864z+1600)(z-1)^7+442368(15-7z)^4(z+1)^7(11z^3-3z^2-2864z-1600)+ \\
& (z^8+2z^7-287z^6-336z^5+9520z^4+3136z^3+108192z^2-529992z-4736)^3 \\
& -5292z^{13}-23814z^{11}-45900z^9-33750z^7+(z^8+4z^7-14z^3+14z^2-20z+25)^3 \\
& -\frac{335544320z^{13}}{1006632960z^{11}}-\frac{45164265472z^9}{167721600z^7}-\frac{27}{167721600z^7}+ \\
& \frac{1}{729}(9z^8+120z^7+940z^6+3240z^5+5670z^4+1288z^3+2700z^2+600z+25)^3 \\
& 1259712(2z+1)^2(7z+8)^4(z^2-18z+297)(z-1)^6-1259712(8-7z)^4(1-2z)^2(z+1)^6(z^2+18z+297)+ \\
& (z^8+24z^7+420z^6+2072z^5+4830z^4-36120z^3+122500z^2-101880z+27945)^3 \\
& 108z^4(z+3)^2(9z^2+42z-5)(1-8z)^6-108(z-3)^2z^4(8z+1)^6(9z^2-42z-5)+(144z^8-1536z^7+5248z^6-5568z^5-720z^4+512z^3+192z^2+24z+1)^3 \\
& -\frac{27}{4}(z+2)^3(z+6)(z^2-2z+2)^2(1-4z)^6+\frac{27}{4}(z-6)(z-2)^3(4z+1)^6(z^2+2z+2)^2+ \\
& (z^8+8z^7+8z^6-24z^5+20z^4+48z^3-16z^2-76z+193)^3 \\
& \frac{1}{64}(432(z-4)^3(-6z^3+22z^2+12z+9)^2z^5-432(z+4)^3(6z^3+22z^2-12z+9)^2z^5+ \\
& 64(z^8+12z^7+48z^6+64z^5+6z^3+22z^2-12z+9)^3 \\
& (z^8-4z^7-98z^6+28z^5+2345z^4+3136z^3-6944z^2+8192z+80128)^3+
\end{aligned}$$

10, 4, 3, 3, 2, 2	$\frac{1728(4-7z)^4(16-3z)^2(z+3)^3(z+11)(z-4)^4-1728(z-11)(z-3)^3(z+4)^4(3z+16)^2(7z+4)^4}{1259712(25-2z)^2(z+1)^2(z^2-14z+25)^3z^4-1259712(z-1)^2(2z+25)^2(z^2+14z+25)^3z^4+}$
9, 9, 2, 2, 1, 1	$\frac{(z^8+40z^7+580z^6+3560z^5+7550z^4-1192z^3-9500z^2-5000z+15625)^3}{729(-16777216(z^2+3)^2(z^2-6z-3)z^9+16777216(z^2+3)^2(z^2+6z-3)z^9+}$
9, 7, 5, 1, 1, 1	$\frac{(z-1)^3(z+3)^3(9z^6+54z^5+27z^4+260z^3-81z^2+486z-243)^3}{729(-64(7z-3)^5(5z^3-51z^2+879z-369)(4z-3)^7+64(4z+3)^7(7z+3)^5(5z^3+51z^2+879z+369)+}$
9, 6, 4, 3, 1, 1	$\frac{(9z^8-144z^7+2268z^6-11872z^5+42070z^4-16464z^3-15876z^2+11232z-1863)^3}{729(64(z-1)^4(4z+5)^3(z^2+4z-20)(14-5z)^6-64(z+1)^4(4z-5)^3(5z+14)^6(z^2-4z-20)-}$
9, 5, 5, 2, 2, 1	$\frac{(z^2-10)^3(-9z^6+270z^4+800z^3+780z^2+672z+1160)^3}{729(64(2z-7)(z^2+5z+7)^2(7z^2-10z-50)^5-64(2z+7)(z^2-5z+7)^2(7z^2+10z-50)^5+}$
9, 5, 3, 3, 1, 1	$\frac{(9z^8-252z^6-224z^5+2478z^4+3920z^3-7700z^2-18000z-4375)^3}{729(-64(z-3)(5z^3-3z-1)^3z^5+64(z+3)(5z^3-3z+1)^3z^5+(z^2+z-1)^3(9z^6+27z^5-5z^3+3z-1)^3)}$
9, 4, 3, 3, 3, 2	$\frac{(z^2-1)^3(4z^3-9z^2-6z-1)^3z^4+64(z+3)^2(4z^3+9z^2-6z+1)^3z^4+}{729(z^2+2z-1)^3(9z^6+54z^5+81z^4-4z^3-9z^2+6z-1)^3)$
8, 8, 4, 2, 1, 1	$\frac{(z^8-4z^6-10z^4+28z^2+1)^3}{-4(3z^2-1)^3(9z^2+24z-11)(1-3z)^8(3z+1)^8(3z^2-24z-11)^3(9z^4+12z^3-1)^3(9z^4+12z^3-36z^2+24z-5)^3}$
8, 8, 3, 3, 1, 1	$\frac{531441}{531441}$
8, 8, 2, 2, 2, 2	$(z^8+z^4+1)^3$
8, 7, 3, 3, 2, 1	$\frac{1}{4096}(108(z-17)^2(3z-2)(7z^2-112z+16)^3(5z-4)^7-108(z+17)^2(3z+2)(5z+4)^7(7z^2+112z+16)^3+}{(16z^8+832z^7+15568z^6+123424z^5+375025z^4+432880z^3+323680z^2+167680z+37120)^3}$
8, 6, 5, 2, 2, 1	$\frac{1}{2985984}(-108(8-15z)^2(7-3z)^2z^5(z+6)(8-7z)^6+108(z-6)z^5(3z+7)^2(7z+8)^6(15z+8)^2+}{(144z^8+192z^7-3248z^6+4704z^5+5145z^4-20384z^3+29568z^2-18432z+4096)^3}$
8, 6, 4, 2, 2, 2	$\frac{432(4-3z)^2(z-1)^4(3z^2+2z+1)^2z^6-432(z+1)^4(9z^3+6z^2-5z+4)^2z^6+64(9z^8+24z^7+16z^6+3z^4+4z^3+1)^3}{46656}$
8, 5, 4, 3, 2, 2	$\frac{1}{64}(-432(z-8)^3(3z+1)^4(-5z^2+42z+9)z^5+432(1-3z)^4(z+8)^3(5z^2+42z-9)^2z^5+}{64(z^8-24z^7+192z^6-512z^5-45z^4+348z^3+328z^2+96z+9)^3}$
8, 4, 4, 4, 3, 1	$\frac{108(z-7)(z-1)^4(z+1)^3(3z^2+2z+1)^4-108(z-1)^3(z+7)(3z^3+z^2-z+1)^4+}{(z^8+8z^7+4z^6-24z^5+18z^4-24z^3+60z^2-24z-3)^3}$
8, 4, 4, 4, 2, 2	$(z^8-4z^6+5z^4-2z^2+1)^3$
7, 7, 7, 1, 1, 1	$51840z^{16}+819072z^{14}+1572480z^{12}+438912z^{10}-6912z^8+(z^8-12z^7+42z^6-56z^5+35z^4-14z^2+4z+1)^3$
7, 6, 6, 2, 2, 1	$46656(z-4)(z^2+5z+13)^2(z^2-3z-3)^6-46656(z+4)(z^2-5z+13)^2(z^2+3z-3)^6+$
7, 6, 5, 4, 1, 1	$\frac{1}{729}(-1728(799-33z)^4(4z+163)^5(3z^2+40z-3416)(z-28)^6+1728(z+28)^6(4z-163)^5(33z+799)^4(3z^2-40z-3416)^3)+$
7, 6, 4, 4, 2, 1	$\frac{(9z^8+48z^7-35000z^6-481152z^5+44788800z^4+967680672z^3-15708981456z^2-549509702400z-3524652257136)^3}{729(108(z+2)^2(12z-25)(3z^2+2z-2)^6-108(z+2)^6(12z+25)(-3z^2+2z+2)^4(z-2)^2+}$

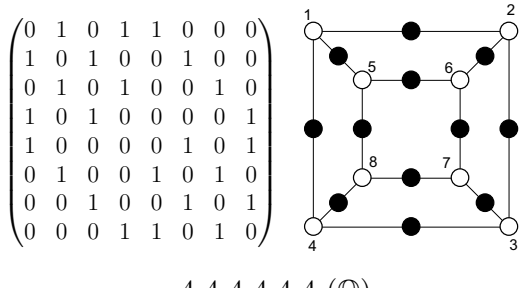
$$\begin{aligned}
 & 7, 5, 5, 3, 2, 2 & 1728(2z+7)^3(z^2-3z+63)^2(3z^2-2z+42)^5-1728(2z-7)^3(z^2+3z+63)^2(3z^2+2z+42)^5+ \\
 & (z^8+84z^6-224z^5+1806z^4-8400z^3+15484z^2+411600z-497007)^3 \\
 & -108z^3(4z-125)(5z^2+10z+14)^4(3z-8)^5+108z^3(3z+8)^5(4z+125)(5z^2-10z+14)^4+ \\
 & (z^8+40z^7+280z^6-280z^5+2660z^4-22288z^3+1120z^2-4160z+10000)^3 \\
 & 7, 5, 4, 4, 3, 1 & \frac{1}{729}(-64(106-9z)^2(z-9)^4(5z^2+12z+12)^3(4z-9)^5+64(z+9)^4(4z+9)^5(9z+106)^2(5z^2-12z+12)^3+ \\
 & (9z^8+288z^7+3192z^6+13216z^5+6720z^4-39648z^3+33264z^2-1041984z+431568)^3) \\
 & 7, 5, 4, 3, 3, 2 & 1728(1-2z)^6z^4(z^2-18z+9)(z-1)^6-1728z^4(z+1)^6(2z+1)^6(z^2+18z+9)+ \\
 & (z^2+6z+3)^3(z^6+18z^5+21z^4+36z^3+39z^2+18z+3)^3 \\
 & 6, 6, 6, 2, 2, 2 & (z^8+12z^6+30z^4-228z^2+9)^3 \\
 & 6, 6, 5, 4, 2, 1 & \frac{729}{4}(z+3)^4(2z+5)^2(4z-15)(z^2-2z-5)^6-\frac{729}{4}(5-2z)^2(z-3)^4(4z+15)(z^2+2z-5)^6+ \\
 & (z^8-30z^6-20z^5+300z^4-24z^3-1430z^2+3300z+9000)^3 \\
 & 6, 6, 5, 3, 3, 1 & -1728(2z-5)(z^2+6z+10)^3(z^2-3z+1)^6+1728(2z+5)(z^2-6z+10)^3(z^2+3z+1)^6+ \\
 & (z^2-5)^3(z^6-15z^4+75z^2+432z-1205)^3 \\
 & 6, 6, 4, 4, 2, 2 & -108(3-2z)^2(z+3)^2(z^2-3)^4(z-1)^6+108(z-3)^2(z+1)^6(2z+3)^2(z^2-3)^4+ \\
 & (z^8-12z^6+8z^5+42z^4-48z^3+28z^2-120z+117)^3 \\
 & 6, 6, 4, 3, 3, 2 & (z^8+4z^6+60z^4+58z^2+1)^3 \\
 & 6, 6, 3, 3, 3 & (z^8-4z^6+6z^4-12z^2+9)^3 \\
 & 6, 5, 4, 4, 3, 2 & \frac{1}{729}(-4((7-2z)^2(3z+2)^3(5z^2-2z+2)^4(z-2)^5+4(z+2)^5(2z+7)^2(3z-2)^3(5z^2+2z+2)^4+ \\
 & (9z^8-72z^7+192z^6-184z^5+20z^4+48z^3+416z^2-256z-48)^3) \\
 & 5, 5, 5, 5, 2, 2 & 1728(2z+5)^5(z^2+5z-25)^2(z^2-6z+10)^5-1728(2z-5)^5(z^2-5z-25)^2(z^2+6z+10)^5+ \\
 & (z^8-60z^6+160z^5+670z^4-10800z^3+59500z^2-130000z+90625)^3 \\
 & 5, 5, 4, 4, 3, 3 & \frac{1}{729}(-4(4z^2-5z+25)^3(9z^2+20z+25)^4(z-1)^5+4(z+1)^5(4z^2+5z+25)^3(9z^2-20z+25)^4+ \\
 & (9z^8+60z^6-40z^5+130z^4-2800z^3+500z^2-5000z+3125)^3) \\
 & 4, 4, 4, 4, 4 & (z^8-14z^4+1)^3
 \end{aligned}$$

Appendix C The Dessin d'Enfant Dataset

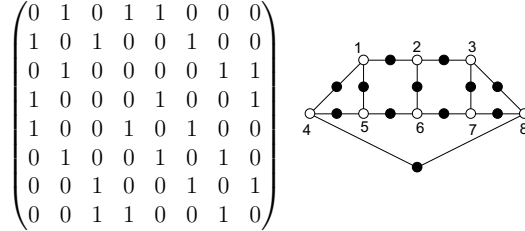
Below the 191 dessins d'enfants, as shown in [14, 34], are presented. Here the white nodes have been arbitrarily labelled from 1 to 8; and the respective adjacency matrices for these labellings are also given. The true dataset used in computation used some (but not all) permutations of these labellings. The dessins are organised with respect to their 6-tuple ramification data, and those with identical 6-tuples are sub-denoted with alphabetic denominations. If these are also isomorphic they are drawn together with the same adjacency matrix.

In addition to the 6-tuple partition of 24 which represents the 6 singular Kodaira fibre types of the corresponding semi-stable elliptically fibred K3 surface, the field which the modular surface's Weierstraß equation is defined over is given in brackets. Where there is no extension \mathbb{Q} is written; where the extension is by roots of a quadratic polynomial one of the roots is given (i.e. \sqrt{a}); and where the extension is by a root of a cubic or quartic polynomial, 'cubic' or 'quartic' are written respectively.

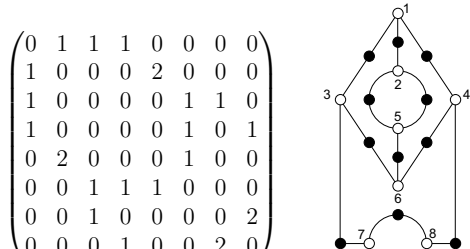
Note that since dessins of the same orbit have the same 6-tuple partition, whilst there may also be multiple orbits with the same 6-part partition, this causes the number of dessins per partition to equal the sum of the degrees of the orbits which share the partition in consideration.



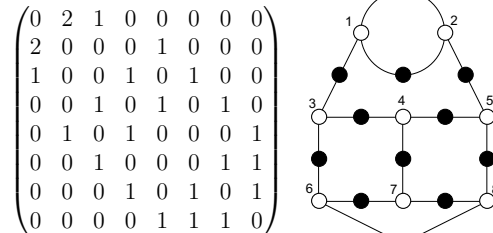
4-4-4-4-4-4 (\mathbb{Q})



5-5-4-4-3-3 (\mathbb{Q})

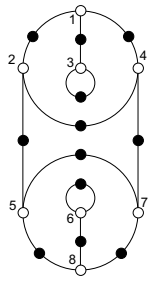


5-5-5-5-2-2 (\mathbb{Q})



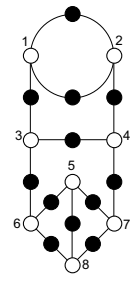
6-5-4-4-3-2 (\mathbb{Q})

$$\begin{pmatrix} 0 & 1 & 1 & 1 & 0 & 0 & 0 & 0 & 0 \\ 1 & 0 & 0 & 1 & 1 & 0 & 0 & 0 & 0 \\ 1 & 0 & 2 & 0 & 0 & 0 & 0 & 0 & 0 \\ 1 & 1 & 0 & 0 & 0 & 0 & 1 & 0 & 0 \\ 0 & 1 & 0 & 0 & 0 & 0 & 1 & 1 & 1 \\ 0 & 0 & 0 & 0 & 0 & 2 & 0 & 1 & 1 \\ 0 & 0 & 0 & 1 & 1 & 0 & 0 & 1 & 1 \\ 0 & 0 & 0 & 0 & 1 & 1 & 1 & 0 & 0 \end{pmatrix}$$



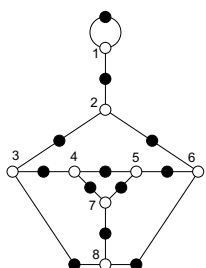
6-6-6-4-1-1 (\mathbb{Q})

$$\begin{pmatrix} 0 & 2 & 1 & 0 & 0 & 0 & 0 & 0 & 0 \\ 2 & 0 & 0 & 1 & 0 & 0 & 0 & 0 & 0 \\ 1 & 0 & 0 & 1 & 0 & 1 & 0 & 0 & 0 \\ 0 & 1 & 1 & 0 & 0 & 0 & 1 & 0 & 0 \\ 0 & 0 & 0 & 0 & 0 & 1 & 1 & 1 & 0 \\ 0 & 0 & 1 & 0 & 1 & 0 & 0 & 1 & 0 \\ 0 & 0 & 0 & 1 & 1 & 0 & 0 & 1 & 0 \\ 0 & 0 & 0 & 0 & 1 & 1 & 1 & 0 & 0 \end{pmatrix}$$



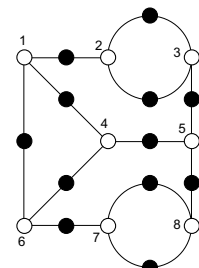
7-5-4-3-3-2 (\mathbb{Q})

$$\begin{pmatrix} 2 & 1 & 0 & 0 & 0 & 0 & 0 & 0 & 0 \\ 1 & 0 & 1 & 0 & 0 & 1 & 0 & 0 & 0 \\ 0 & 1 & 0 & 1 & 0 & 0 & 0 & 1 & 0 \\ 0 & 0 & 1 & 0 & 1 & 0 & 1 & 0 & 0 \\ 0 & 0 & 0 & 1 & 0 & 1 & 1 & 0 & 0 \\ 0 & 1 & 0 & 0 & 1 & 0 & 0 & 1 & 0 \\ 0 & 0 & 0 & 1 & 1 & 0 & 0 & 0 & 1 \\ 0 & 0 & 1 & 0 & 0 & 1 & 1 & 0 & 0 \end{pmatrix}$$



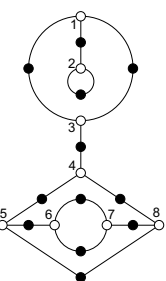
7-5-4-4-3-1 (\mathbb{Q})

$$\begin{pmatrix} 0 & 1 & 0 & 1 & 0 & 1 & 0 & 0 \\ 1 & 0 & 2 & 0 & 0 & 0 & 0 & 0 \\ 0 & 2 & 0 & 0 & 1 & 0 & 0 & 0 \\ 1 & 0 & 0 & 0 & 1 & 1 & 0 & 0 \\ 0 & 0 & 1 & 1 & 0 & 0 & 0 & 1 \\ 1 & 0 & 0 & 1 & 0 & 0 & 1 & 0 \\ 0 & 0 & 0 & 0 & 0 & 1 & 0 & 2 \\ 0 & 0 & 0 & 0 & 1 & 0 & 2 & 0 \end{pmatrix}$$



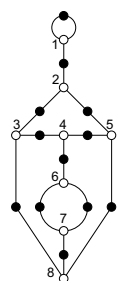
7-5-5-3-2-2 (\mathbb{Q})

$$\begin{pmatrix} 0 & 1 & 2 & 0 & 0 & 0 & 0 & 0 & 0 \\ 1 & 2 & 0 & 0 & 0 & 0 & 0 & 0 & 0 \\ 2 & 0 & 0 & 1 & 0 & 0 & 0 & 0 & 0 \\ 0 & 0 & 1 & 0 & 1 & 0 & 0 & 1 & 0 \\ 0 & 0 & 0 & 1 & 0 & 1 & 0 & 0 & 1 \\ 0 & 0 & 0 & 0 & 1 & 0 & 2 & 0 & 0 \\ 0 & 0 & 0 & 0 & 0 & 0 & 2 & 0 & 1 \\ 0 & 0 & 0 & 1 & 1 & 0 & 1 & 0 & 0 \end{pmatrix}$$



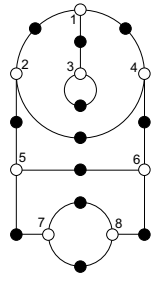
7-5-5-4-2-1 A ($\sqrt{2}$)

$$\begin{pmatrix} 2 & 1 & 0 & 0 & 0 & 0 & 0 & 0 & 0 \\ 1 & 0 & 1 & 0 & 1 & 0 & 0 & 0 & 0 \\ 0 & 1 & 0 & 1 & 0 & 0 & 0 & 0 & 1 \\ 0 & 0 & 1 & 0 & 1 & 1 & 0 & 0 & 0 \\ 0 & 1 & 0 & 1 & 0 & 0 & 0 & 0 & 1 \\ 0 & 0 & 0 & 1 & 0 & 0 & 2 & 0 & 0 \\ 0 & 0 & 0 & 0 & 0 & 2 & 0 & 1 & 0 \\ 0 & 0 & 1 & 0 & 1 & 0 & 1 & 0 & 0 \end{pmatrix}$$



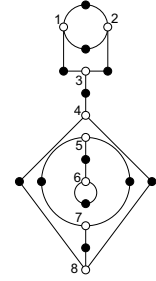
7-5-5-4-2-1 B $(\sqrt{2})$

$$\begin{pmatrix} 0 & 1 & 1 & 1 & 0 & 0 & 0 & 0 \\ 1 & 0 & 0 & 1 & 1 & 0 & 0 & 0 \\ 1 & 0 & 2 & 0 & 0 & 0 & 0 & 0 \\ 1 & 1 & 0 & 0 & 0 & 1 & 0 & 0 \\ 0 & 1 & 0 & 0 & 0 & 1 & 1 & 0 \\ 0 & 0 & 0 & 1 & 1 & 0 & 0 & 1 \\ 0 & 0 & 0 & 0 & 1 & 0 & 0 & 2 \\ 0 & 0 & 0 & 0 & 0 & 1 & 2 & 0 \end{pmatrix}$$



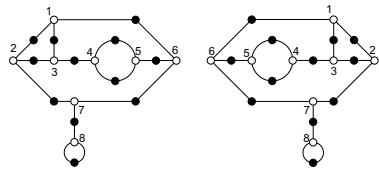
7-6-4-4-2-1 (\mathbb{Q})

$$\begin{pmatrix} 0 & 2 & 1 & 0 & 0 & 0 & 0 & 0 & 0 \\ 2 & 0 & 1 & 0 & 0 & 0 & 0 & 0 & 0 \\ 1 & 1 & 0 & 1 & 0 & 0 & 0 & 0 & 0 \\ 0 & 0 & 1 & 0 & 0 & 0 & 0 & 2 & 0 \\ 0 & 0 & 0 & 0 & 0 & 1 & 2 & 0 & 0 \\ 0 & 0 & 0 & 0 & 1 & 2 & 0 & 0 & 0 \\ 0 & 0 & 0 & 0 & 2 & 0 & 0 & 1 & 0 \\ 0 & 0 & 0 & 2 & 0 & 0 & 1 & 0 & 0 \end{pmatrix}$$



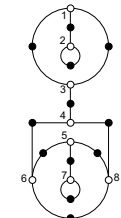
7-6-5-3-2-1 A (cubic)

$$\begin{pmatrix} 0 & 1 & 1 & 0 & 0 & 1 & 0 & 0 \\ 1 & 0 & 1 & 0 & 0 & 0 & 1 & 0 \\ 1 & 1 & 0 & 1 & 0 & 0 & 0 & 0 \\ 0 & 0 & 1 & 0 & 2 & 0 & 0 & 0 \\ 0 & 0 & 0 & 2 & 0 & 1 & 0 & 0 \\ 1 & 0 & 0 & 0 & 1 & 0 & 1 & 0 \\ 0 & 1 & 0 & 0 & 0 & 1 & 0 & 1 \\ 0 & 0 & 0 & 0 & 0 & 0 & 1 & 2 \end{pmatrix}$$



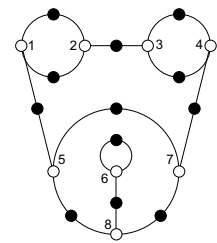
7-6-5-3-2-1 B & C (cubic)

$$\begin{pmatrix} 0 & 1 & 2 & 0 & 0 & 0 & 0 & 0 \\ 1 & 2 & 0 & 0 & 0 & 0 & 0 & 0 \\ 2 & 0 & 0 & 1 & 0 & 0 & 0 & 0 \\ 0 & 0 & 1 & 0 & 0 & 1 & 0 & 1 \\ 0 & 0 & 0 & 0 & 0 & 1 & 1 & 1 \\ 0 & 0 & 0 & 1 & 1 & 0 & 0 & 1 \\ 0 & 0 & 0 & 0 & 1 & 0 & 2 & 0 \\ 0 & 0 & 0 & 1 & 1 & 1 & 0 & 0 \end{pmatrix}$$



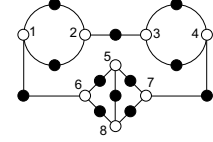
7-6-5-4-1-1 (\mathbb{Q})

$$\begin{pmatrix} 0 & 2 & 0 & 0 & 1 & 0 & 0 & 0 \\ 2 & 0 & 1 & 0 & 0 & 0 & 0 & 0 \\ 0 & 1 & 0 & 2 & 0 & 0 & 0 & 0 \\ 0 & 0 & 2 & 0 & 0 & 0 & 1 & 0 \\ 1 & 0 & 0 & 0 & 0 & 0 & 1 & 1 \\ 0 & 0 & 0 & 0 & 0 & 2 & 0 & 1 \\ 0 & 0 & 0 & 1 & 1 & 0 & 0 & 1 \\ 0 & 0 & 0 & 0 & 1 & 1 & 1 & 0 \end{pmatrix}$$



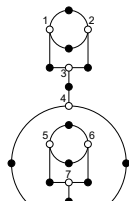
7-6-6-2-2-1 (\mathbb{Q})

$$\begin{pmatrix} 0 & 2 & 0 & 0 & 0 & 1 & 0 & 0 \\ 2 & 0 & 1 & 0 & 0 & 0 & 0 & 0 \\ 0 & 1 & 0 & 2 & 0 & 0 & 0 & 0 \\ 0 & 0 & 2 & 0 & 0 & 0 & 1 & 0 \\ 0 & 0 & 0 & 0 & 0 & 1 & 1 & 1 \\ 1 & 0 & 0 & 0 & 1 & 0 & 0 & 1 \\ 0 & 0 & 0 & 1 & 1 & 0 & 0 & 1 \\ 0 & 0 & 0 & 0 & 1 & 1 & 1 & 0 \end{pmatrix}$$



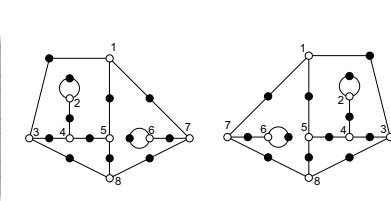
7-7-3-3-2-2 A ($\sqrt{7}$)

$$\begin{pmatrix} 0 & 2 & 1 & 0 & 0 & 0 & 0 & 0 \\ 2 & 0 & 1 & 0 & 0 & 0 & 0 & 0 \\ 1 & 1 & 0 & 1 & 0 & 0 & 0 & 0 \\ 0 & 0 & 1 & 0 & 0 & 0 & 2 & 0 \\ 0 & 0 & 0 & 0 & 0 & 2 & 1 & 0 \\ 0 & 0 & 0 & 0 & 2 & 0 & 1 & 0 \\ 0 & 0 & 0 & 0 & 1 & 1 & 0 & 1 \\ 0 & 0 & 0 & 2 & 0 & 0 & 1 & 0 \end{pmatrix}$$



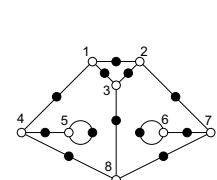
7-7-3-3-2-2 B ($\sqrt{7}$)

$$\begin{pmatrix} 0 & 0 & 1 & 0 & 1 & 0 & 1 & 0 \\ 0 & 2 & 0 & 1 & 0 & 0 & 0 & 0 \\ 1 & 0 & 0 & 1 & 0 & 0 & 0 & 1 \\ 0 & 1 & 1 & 0 & 1 & 0 & 0 & 0 \\ 1 & 0 & 0 & 1 & 0 & 0 & 0 & 1 \\ 0 & 0 & 0 & 0 & 0 & 2 & 1 & 0 \\ 1 & 0 & 0 & 0 & 0 & 1 & 0 & 1 \\ 0 & 0 & 1 & 0 & 1 & 0 & 1 & 0 \end{pmatrix}$$



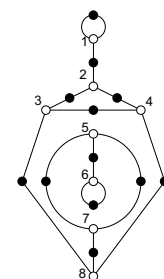
7-7-4-4-1-1 A & B ($\sqrt{-7}$)

$$\begin{pmatrix} 0 & 1 & 1 & 1 & 0 & 0 & 0 & 0 \\ 1 & 0 & 1 & 0 & 0 & 0 & 1 & 0 \\ 1 & 1 & 0 & 0 & 0 & 0 & 0 & 1 \\ 1 & 0 & 0 & 0 & 1 & 0 & 0 & 1 \\ 0 & 0 & 0 & 1 & 2 & 0 & 0 & 0 \\ 0 & 0 & 0 & 0 & 0 & 2 & 1 & 0 \\ 0 & 1 & 0 & 0 & 0 & 1 & 0 & 1 \\ 0 & 0 & 1 & 1 & 0 & 0 & 1 & 0 \end{pmatrix}$$



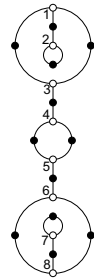
7-7-5-3-1-1 A ($\sqrt{21}$)

$$\begin{pmatrix} 2 & 1 & 0 & 0 & 0 & 0 & 0 & 0 \\ 1 & 0 & 1 & 1 & 0 & 0 & 0 & 0 \\ 0 & 1 & 0 & 1 & 0 & 0 & 0 & 1 \\ 0 & 1 & 1 & 0 & 0 & 0 & 0 & 1 \\ 0 & 0 & 0 & 0 & 0 & 1 & 2 & 0 \\ 0 & 0 & 0 & 0 & 1 & 2 & 0 & 0 \\ 0 & 0 & 0 & 0 & 2 & 0 & 0 & 1 \\ 0 & 0 & 1 & 1 & 0 & 0 & 1 & 0 \end{pmatrix}$$



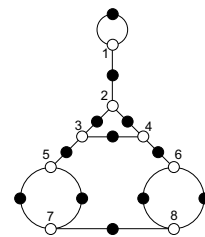
7-7-5-3-1-1 B ($\sqrt{21}$)

$$\begin{pmatrix} 0 & 1 & 2 & 0 & 0 & 0 & 0 & 0 \\ 1 & 2 & 0 & 0 & 0 & 0 & 0 & 0 \\ 2 & 0 & 0 & 1 & 0 & 0 & 0 & 0 \\ 0 & 0 & 1 & 0 & 2 & 0 & 0 & 0 \\ 0 & 0 & 0 & 2 & 0 & 1 & 0 & 0 \\ 0 & 0 & 0 & 0 & 1 & 0 & 0 & 2 \\ 0 & 0 & 0 & 0 & 0 & 0 & 2 & 1 \\ 0 & 0 & 0 & 0 & 0 & 2 & 1 & 0 \end{pmatrix}$$



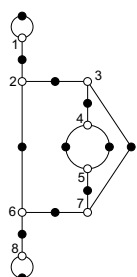
10-5-5-2-1-1 B $(\sqrt{5})$

$$\begin{pmatrix} 2 & 1 & 0 & 0 & 0 & 0 & 0 & 0 & 0 \\ 1 & 0 & 1 & 1 & 0 & 0 & 0 & 0 & 0 \\ 0 & 1 & 0 & 1 & 1 & 0 & 0 & 0 & 0 \\ 0 & 1 & 1 & 0 & 0 & 1 & 0 & 0 & 0 \\ 0 & 0 & 1 & 0 & 0 & 0 & 2 & 0 & 0 \\ 0 & 0 & 0 & 1 & 0 & 0 & 0 & 2 & 0 \\ 0 & 0 & 0 & 0 & 2 & 0 & 0 & 1 & 0 \\ 0 & 0 & 0 & 0 & 0 & 2 & 1 & 0 & 0 \end{pmatrix}$$



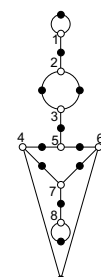
10-6-3-2-2-1 (\mathbb{Q})

$$\begin{pmatrix} 2 & 1 & 0 & 0 & 0 & 0 & 0 & 0 & 0 \\ 1 & 0 & 1 & 0 & 0 & 1 & 0 & 0 & 0 \\ 0 & 1 & 0 & 1 & 0 & 0 & 1 & 0 & 0 \\ 0 & 0 & 1 & 0 & 2 & 0 & 0 & 0 & 0 \\ 0 & 0 & 0 & 2 & 0 & 0 & 1 & 0 & 0 \\ 0 & 1 & 0 & 0 & 0 & 0 & 1 & 1 & 0 \\ 0 & 0 & 1 & 0 & 1 & 1 & 0 & 0 & 0 \\ 0 & 0 & 0 & 0 & 0 & 1 & 0 & 2 & 0 \end{pmatrix}$$



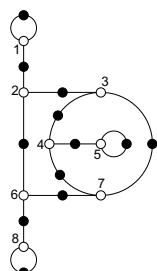
10-6-4-2-1-1 A (\mathbb{Q})

$$\begin{pmatrix} 2 & 1 & 0 & 0 & 0 & 0 & 0 & 0 \\ 1 & 0 & 2 & 0 & 0 & 0 & 0 & 0 \\ 0 & 2 & 0 & 0 & 1 & 0 & 0 & 0 \\ 0 & 0 & 0 & 0 & 1 & 1 & 1 & 0 \\ 0 & 0 & 1 & 1 & 0 & 1 & 0 & 0 \\ 0 & 0 & 0 & 1 & 1 & 0 & 1 & 0 \\ 0 & 0 & 0 & 1 & 0 & 1 & 0 & 1 \\ 0 & 0 & 0 & 0 & 0 & 0 & 1 & 2 \end{pmatrix}$$



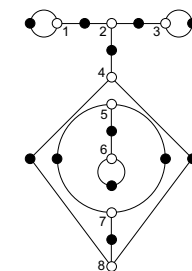
10-6-4-2-1-1 B (\mathbb{Q})

$$\begin{pmatrix} 2 & 1 & 0 & 0 & 0 & 0 & 0 & 0 \\ 1 & 0 & 1 & 0 & 0 & 1 & 0 & 0 \\ 0 & 1 & 0 & 1 & 0 & 0 & 1 & 0 \\ 0 & 0 & 1 & 0 & 1 & 0 & 1 & 0 \\ 0 & 0 & 0 & 1 & 2 & 0 & 0 & 0 \\ 0 & 1 & 0 & 0 & 0 & 0 & 1 & 1 \\ 0 & 0 & 1 & 1 & 0 & 1 & 0 & 0 \\ 0 & 0 & 0 & 0 & 0 & 1 & 0 & 2 \end{pmatrix}$$



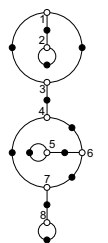
10-6-5-1-1-1 A (Q)

$$\begin{pmatrix} 2 & 1 & 0 & 0 & 0 & 0 & 0 & 0 & 0 \\ 1 & 0 & 1 & 1 & 0 & 0 & 0 & 0 & 0 \\ 0 & 1 & 2 & 0 & 0 & 0 & 0 & 0 & 0 \\ 0 & 1 & 0 & 0 & 0 & 0 & 0 & 0 & 2 \\ 0 & 0 & 0 & 0 & 0 & 1 & 2 & 0 & 0 \\ 0 & 0 & 0 & 0 & 1 & 2 & 0 & 0 & 0 \\ 0 & 0 & 0 & 0 & 2 & 0 & 0 & 1 & 1 \\ 0 & 0 & 0 & 2 & 0 & 0 & 1 & 0 & 0 \end{pmatrix}$$



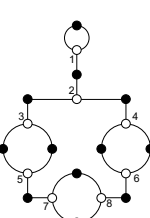
10-6-5-1-1-1 B (cubic)

$$\begin{pmatrix} 0 & 1 & 2 & 0 & 0 & 0 & 0 & 0 & 0 \\ 1 & 2 & 0 & 0 & 0 & 0 & 0 & 0 & 0 \\ 2 & 0 & 0 & 1 & 0 & 0 & 0 & 0 & 0 \\ 0 & 0 & 1 & 0 & 0 & 1 & 1 & 0 & 0 \\ 0 & 0 & 0 & 0 & 2 & 1 & 0 & 0 & 0 \\ 0 & 0 & 0 & 1 & 1 & 0 & 1 & 0 & 0 \\ 0 & 0 & 0 & 1 & 0 & 1 & 0 & 1 & 1 \\ 0 & 0 & 0 & 0 & 0 & 0 & 1 & 2 & 0 \end{pmatrix}$$



10-6-5-1-1-1 C & D (cubic)

$$\begin{pmatrix} 2 & 1 & 0 & 0 & 0 & 0 & 0 & 0 & 0 \\ 1 & 0 & 1 & 1 & 0 & 0 & 0 & 0 & 0 \\ 0 & 1 & 0 & 0 & 2 & 0 & 0 & 0 & 0 \\ 0 & 1 & 0 & 0 & 0 & 2 & 0 & 0 & 0 \\ 0 & 0 & 2 & 0 & 0 & 0 & 1 & 0 & 0 \\ 0 & 0 & 0 & 2 & 0 & 0 & 0 & 1 & 0 \\ 0 & 0 & 0 & 0 & 1 & 0 & 0 & 2 & 0 \\ 0 & 0 & 0 & 0 & 0 & 1 & 2 & 0 & 0 \end{pmatrix}$$



10-7-2-2-2-1 (\mathbb{Q})

$$\left(\begin{array}{ccccccc} 2 & 1 & 0 & 0 & 0 & 0 & 0 \\ 1 & 0 & 1 & 1 & 0 & 0 & 0 \\ 0 & 1 & 2 & 0 & 0 & 0 & 0 \\ 0 & 1 & 0 & 0 & 0 & 0 & 2 \\ 0 & 0 & 0 & 0 & 0 & 2 & 1 \\ 0 & 0 & 0 & 0 & 2 & 0 & 1 \\ 0 & 0 & 0 & 0 & 1 & 1 & 0 \\ 0 & 0 & 0 & 2 & 0 & 0 & 1 \end{array} \right)$$

$$10-7-3-2-1-1 \text{ A } (\sqrt{21})$$

$$\left(\begin{array}{cccccccc} 0 & 1 & 1 & 0 & 1 & 0 & 0 & 0 \\ 1 & 0 & 1 & 1 & 0 & 0 & 0 & 0 \\ 1 & 1 & 0 & 0 & 1 & 0 & 0 & 0 \\ 0 & 1 & 0 & 2 & 0 & 0 & 0 & 0 \\ 1 & 0 & 1 & 0 & 0 & 1 & 0 & 0 \\ 0 & 0 & 0 & 0 & 1 & 0 & 2 & 0 \\ 0 & 0 & 0 & 0 & 0 & 2 & 0 & 1 \\ 0 & 0 & 0 & 0 & 0 & 0 & 1 & 2 \end{array} \right)$$

10-7-3-2-1-1 B $(\sqrt{21})$

$$\begin{pmatrix} 2 & 1 & 0 & 0 & 0 & 0 & 0 & 0 \\ 1 & 0 & 1 & 0 & 1 & 0 & 0 & 0 \\ 0 & 1 & 0 & 0 & 0 & 1 & 1 & 0 \\ 0 & 0 & 0 & 2 & 0 & 1 & 0 & 0 \\ 0 & 1 & 0 & 0 & 0 & 1 & 1 & 0 \\ 0 & 0 & 1 & 1 & 1 & 0 & 0 & 0 \\ 0 & 0 & 1 & 0 & 1 & 0 & 0 & 1 \\ 0 & 0 & 0 & 0 & 0 & 0 & 1 & 2 \end{pmatrix}$$

10-7-4-1-1-1 (\mathbb{Q})

$$\left(\begin{array}{cccccccc} 2 & 1 & 0 & 0 & 0 & 0 & 0 & 0 \\ 1 & 0 & 1 & 0 & 0 & 1 & 0 & 0 \\ 0 & 1 & 0 & 0 & 1 & 0 & 1 & 0 \\ 0 & 0 & 0 & 2 & 1 & 0 & 0 & 0 \\ 0 & 0 & 1 & 1 & 0 & 0 & 1 & 0 \\ 0 & 1 & 0 & 0 & 0 & 0 & 1 & 1 \\ 0 & 0 & 1 & 0 & 1 & 1 & 0 & 0 \\ 0 & 0 & 0 & 0 & 0 & 1 & 0 & 2 \end{array} \right)$$

10-8-3-1-1-1 (\mathbb{Q})

$$\begin{pmatrix}
 2 & 1 & 0 & 0 & 0 & 0 & 0 & 0 \\
 1 & 0 & 1 & 1 & 0 & 0 & 0 & 0 \\
 0 & 1 & 2 & 0 & 0 & 0 & 0 & 0 \\
 0 & 1 & 0 & 0 & 0 & 0 & 0 & 2 \\
 0 & 0 & 0 & 0 & 2 & 1 & 0 & 0 \\
 0 & 0 & 0 & 0 & 1 & 0 & 2 & 0 \\
 0 & 0 & 0 & 0 & 0 & 2 & 0 & 1 \\
 0 & 0 & 0 & 2 & 0 & 0 & 1 & 0
 \end{pmatrix}$$

10-9-2-1-1-1 A ($\sqrt{5}$)

$$\begin{pmatrix} 2 & 1 & 0 & 0 & 0 & 0 & 0 & 0 \\ 1 & 0 & 2 & 0 & 0 & 0 & 0 & 0 \\ 0 & 2 & 0 & 1 & 0 & 0 & 0 & 0 \\ 0 & 0 & 1 & 0 & 0 & 0 & 1 & 1 \\ 0 & 0 & 0 & 0 & 2 & 0 & 1 & 0 \\ 0 & 0 & 0 & 0 & 0 & 2 & 0 & 1 \\ 0 & 0 & 0 & 1 & 1 & 0 & 0 & 1 \\ 0 & 0 & 0 & 1 & 0 & 1 & 1 & 0 \end{pmatrix}$$

10-9-2-1-1-1 B ($\sqrt{5}$)

10-10-1-1-1-1 A & B ($\sqrt{5}$)

10-10-1-1-1-1 C (\mathbb{Q})

$$\left(\begin{array}{ccccccc} 2 & 1 & 0 & 0 & 0 & 0 & 0 \\ 1 & 0 & 1 & 0 & 1 & 0 & 0 \\ 0 & 1 & 0 & 1 & 0 & 1 & 0 \\ 0 & 0 & 1 & 0 & 0 & 0 & 2 \\ 0 & 1 & 0 & 0 & 0 & 1 & 0 \\ 0 & 0 & 1 & 0 & 1 & 0 & 1 \\ 0 & 0 & 0 & 2 & 0 & 1 & 0 \\ 0 & 0 & 0 & 0 & 1 & 0 & 0 \\ \end{array} \right)$$

12-4-4-2-1-1 (\mathbb{Q})

$$\begin{pmatrix} 2 & 1 & 0 & 0 & 0 & 0 & 0 & 0 \\ 1 & 0 & 2 & 0 & 0 & 0 & 0 & 0 \\ 0 & 2 & 0 & 1 & 0 & 0 & 0 & 0 \\ 0 & 0 & 1 & 0 & 1 & 1 & 0 & 0 \\ 0 & 0 & 0 & 1 & 0 & 0 & 2 & 0 \\ 0 & 0 & 0 & 1 & 0 & 0 & 0 & 2 \\ 0 & 0 & 0 & 0 & 2 & 0 & 0 & 1 \\ 0 & 0 & 0 & 0 & 0 & 2 & 1 & 0 \end{pmatrix}$$

12-5-2-2-2-1 (\mathbb{Q})

12-5-3-2-1-1 A & B (quartic)

12-5-3-2-1-1 C & D (quartic)

$$\left(\begin{array}{cccccccc} 2 & 1 & 0 & 0 & 0 & 0 & 0 & 0 \\ 1 & 0 & 1 & 1 & 0 & 0 & 0 & 0 \\ 0 & 1 & 0 & 0 & 2 & 0 & 0 & 0 \\ 0 & 1 & 0 & 0 & 0 & 2 & 0 & 0 \\ 0 & 0 & 2 & 0 & 0 & 0 & 1 & 0 \\ 0 & 0 & 0 & 2 & 0 & 0 & 1 & 0 \\ 0 & 0 & 0 & 0 & 1 & 1 & 0 & 1 \\ 0 & 0 & 0 & 0 & 0 & 0 & 1 & 2 \end{array} \right)$$

12-6-2-2-1-1 A (\mathbb{Q})

$$\left(\begin{array}{ccccccc} 0 & 1 & 0 & 2 & 0 & 0 & 0 \\ 1 & 0 & 1 & 0 & 0 & 0 & 1 \\ 0 & 1 & 2 & 0 & 0 & 0 & 0 \\ 2 & 0 & 0 & 0 & 1 & 0 & 0 \\ 0 & 0 & 0 & 1 & 0 & 2 & 0 \\ 0 & 0 & 0 & 0 & 2 & 0 & 1 \\ 0 & 1 & 0 & 0 & 0 & 1 & 0 \\ 0 & 0 & 0 & 0 & 0 & 0 & 1 \end{array} \right)$$

12-6-2-2-1-1 B (\mathbb{Q})

$$\left(\begin{array}{ccccccc} 2 & 1 & 0 & 0 & 0 & 0 & 0 \\ 1 & 0 & 1 & 1 & 0 & 0 & 0 \\ 0 & 1 & 2 & 0 & 0 & 0 & 0 \\ 0 & 1 & 0 & 0 & 1 & 0 & 1 \\ 0 & 0 & 0 & 1 & 0 & 0 & 1 \\ 0 & 0 & 0 & 0 & 0 & 2 & 0 \\ 0 & 0 & 0 & 1 & 1 & 0 & 0 \\ 0 & 0 & 0 & 1 & 1 & 1 & 0 \end{array} \right)$$

12-6-3-1-1-1 (\mathbb{Q})

12-7-2-1-1-1 A & B ($\sqrt{-3}$)

References

- [1] Belyi, G.V. (1980). On Galois Extensons of a Maximal Cyclotomic Field. *Mathematics of the USSR-Izvestiya*. **14** (2), 247.
- [2] Grothendieck, A. (1984). *Esquisse d'un Programme*. Available from: <https://webusers.imj-prg.fr/~leila.schneps/grothendieckcircle/EsquisseFr.pdf>
- [3] Klein, F. (1879). Ueber die Transformation elfter Ordnung der elliptischen Functionen, *Mathematische Annalen*, **15** (3 - 4): 533 - 555.
- [4] Girondo, E., González-Diez, G. (2011). *Introduction to Compact Riemann Surfaces and Dessins d'Enfants* (London Mathematical Society Student Texts). Cambridge: Cambridge University Press. doi:10.1017/CBO9781139048910
- [5] Guillot, P. (2014). *An Elementary Approach to Dessin d'Enfants and the Grothendieck-Teichmüller Group*. [arXiv:math/1309.1968 [math]].
- [6] Lando, S.K., Zvonkin, A.K., Gamkrelidze, R.V. (ed.), Vassiliev, V.A. (ed.) (2004). *Graphs on Surfaces and Their Applications*. Encyclopaedia of Mathematical Sciences, 141. Heidelberg, Springer.
- [7] Zapponi, L. (2003). What is a... Dessin D'Enfant. *Notices of the AMS*. **50** (7) 788-789. Available from: <https://www.ams.org/notices/200307/what-is.pdf>
- [8] Ashok, S.K., Cachazo, F., Dell'Aquila, E. (2007). Children's drawings from Seiberg-Witten curves. *Commun. Num. Theor. Phys.* **1**, 237-305. [arXiv:hep-th/0611082 [hep-th]].
- [9] Seiberg, N., Witten, E. (1994). Electric - magnetic duality, monopole condensation, and confinement in $N=2$ supersymmetric Yang-Mills theory. *Nucl. Phys. B* **426**, 19-52. [arXiv:hep-th/9407087 [hep-th]].
- [10] Jejjala, V., Ramgoolam, S., Rodriguez-Gomez, D. (2011). Toric CFTs, Permutation Triples and Belyi Pairs. *JHEP* **03**, 065. [arXiv:1012.2351 [hep-th]].
- [11] Hanany, A., He, Y., Jejjala, V., Pasukonis, J., Ramgoolam, S., Rodriguez-Gomez, D. (2011) The Beta Ansatz: A Tale of Two Complex Structures. *JHEP* **06**, 056. [arXiv:1104.5490 [hep-th]].
- [12] He, Y., Hu, Z., Probst, M., Read, J. (2018). YangMills theory and the ABC conjecture. *Int. J. Mod. Phys. A* **33**, no.13, 1850053. [arXiv:1602.01780 [hep-th]].
- [13] Franco, S., Hanany, A., Martelli, D., Sparks, J., Vegh, D., Wecht, B. (2006). Gauge theories from toric geometry and brane tilings. *JHEP* **01**, 128. [arXiv:hep-th/0505211 [hep-th]].
- [14] He, Y., McKay, J., Read, J. (2013). Modular Subgroups, Dessins d'Enfants and Elliptic K3 Surfaces. *J. Comput. Math.* **16**, 271-318. [arXiv:1211.1931 [math.AG]].

[15] He, Y., McKay, J. (2013). N=2 Gauge Theories: Congruence Subgroups, Coset Graphs and Modular Surfaces. *J. Math. Phys.* **54**, 012301. [arXiv:1201.3633 [hep-th]].

[16] Gaiotto, D. (2012). N=2 dualities. *JHEP* **08**, 034. [arXiv:0904.2715 [hep-th]].

[17] Vidunas, R., He, Y. (2017). Genus One Belyi Maps by Quadratic Correspondences. *Int. J. of Mathematics*, **June 2017**. [arXiv:1706.04258 [math.AG]].

[18] He, Y. (2017). *Deep-Learning the Landscape*. [arXiv:1706.02714 [hep-th]]. Machine-learning the string landscape *Phys. Lett. B* **774**, 564-568.

[19] Krefl, D., Seong, R.K. (2017). Machine Learning of Calabi-Yau Volumes. *Phys. Rev. D* **96**, no. 6, 066014. [arXiv:1706.03346 [hep-th]].

[20] Ruehle, F. (2017). Evolving neural networks with genetic algorithms to study the String Landscape. *JHEP* **08**, 038. [arXiv:1706.07024 [hep-th]].

[21] Carifio, J., Halverson, J., Krioukov, D., Nelson, B.D. (2017). Machine Learning in the String Landscape. *JHEP* **1709**, 157. [arXiv:1707.00655 [hep-th]].

[22] He, Y. (2018). *The Calabi-Yau Landscape: from Geometry, to Physics, to Machine-Learning*. [arXiv:1812.02893 [hep-th]].

[23] Ruehle, F. (2020). Data science applications to string theory. *Phys. Rept.* **839**, 1-117.

[24] Bao, J., He, Y., Hirst, E., Pietromonaco, S. (2020). *Lectures on the Calabi-Yau Landscape*. [arXiv:2001.01212 [hep-th]].

[25] He, Y., *Machine-Learning Mathematical Structures*. Oxford ML Physics Seminar Series, <https://www.youtube.com/watch?v=nMP2f14gYzc>.

[26] Ashmore, A., He, Y., Ovrut, B.A. (2019). Machine learning Calabi-Yau metrics. [arXiv:1910.08605 [hep-th]].

[27] Bull, K., He, Y., Jejjala, V., Mishra, C. (2018). Machine Learning CICY Threefolds. *Phys. Lett. B* **785**, 65-72. [arXiv:1806.03121 [hep-th]].

[28] Brodie, C.R., Constantin, A., Deen, R., Lukas, A. (2020). Machine Learning Line Bundle Cohomology. *Fortsch. Phys.* **68**, no.1, 1900087. [arXiv:1906.08730 [hep-th]].

[29] He, Y., Kim, M. (2019). *Learning Algebraic Structures: Preliminary Investigations*. [arXiv:1905.02263 [cs.LG]].

[30] Bao, J., Franco, S., He, Y., Hirst, E., Musiker, G., Xiao, Y. *Machine-Learning Quiver Gauge Theories*, to appear.

[31] He, Y., Yau, S.T. *Graph Laplacians, Riemannian Manifolds and Machine-Learning*, to appear.

[32] Alessandretti, L., Baronchelli, A., He, Y. (2019). *Machine Learning meets Number Theory: The Data Science of Birch-Swinnerton-Dyer*. [arXiv:1911.02008 [math.NT]].

[33] Miranda, R., Persson, U., (1989). Configurations of In Fibers on Elliptic K3-Surfaces. *Mathematische Zeitschrift*. **201** (3), 339361.

[34] Beukers, F., Montanus, H. (2008). Explicit calculation of elliptic fibrations of K3-surfaces and their Belyi-maps. Number theory and polynomials, *LMS Lecture Note Series*, **352**, 33-51. CUP. Dessins Coming from the Miranda-Persson Table. Available from: http://www.staff.science.uu.nl/~beuke106/MirandaPersson_table/Dessins.html

[35] Sebbar, A. (2001). Classification of Torsion-Free Genus zero Congruence Groups. *American Mathematical Society*. **129** (9), 2517-2527. Available from: <https://www.ams.org/journals/proc/2001-129-09/S0002-9939-01-06176-7/S0002-9939-01-06176-7.pdf>

[36] McKay, J., Sebbar, A. (2001). J-Invariants of Arithmetic Semistable Elliptic Surfaces and Graphs. In: *Proceedings on Moonshine and related topics* Montreal, QC, AMS pp. 119130.

[37] He, Y., Read, J. (2015). Dessins denfants in $\mathcal{N} = 2$ generalised quiver theories. *JHEP* **08**, 085. [arXiv:1503.06418 [hep-th]].

[38] Beukers, F. (n.d.) *montanuslist.txt*. Available from: <https://www.staff.science.uu.nl/~beuke106/mirandapersson/montanuslist.txt>

[39] Edwards, H.M. (1984). *A Note on Galois Theory*. Archive for History of Exact Sciences, **41** (2), 1990, pp. 163169. JSTOR, www.jstor.org/stable/41133884

[40] Cox, D.A. (2012). *Galois Theory*. Hoboken, New Jersey, John Wiley & Sons, Inc.

[41] Shimura, G. (1971). *Introduction to the Arithmetic Theory of Automorphic Functions*. Princeton University Press, New Jersey.

[42] Hanany, A., He, Y., Jejjala, V., Pasukonis, J., Ramgoolam, S., Rodriguez-Gomez, D. (2012). Invariants of Toric Seiberg Duality. *Int. J. Mod. Phys. A* **27**, 1250002. [arXiv:1107.4101 [hep-th]].

[43] Tachikawa, Y. (2014). *$N = 2$ supersymmetric dynamics for pedestrians*. Springer International Publishing. Available from: <https://www.springer.com/gp/book/9783319088211>

[44] Cachazo, F., Seiberg, N., Witten, E. (2003). *Phases of $N=1$ Supersymmetric Gauge Theories and Matrices*. [arXiv:hep-th/0301006 [hep-th]].

[45] Sun, C., Shrivastava, A., Singh, S., Gupta., A. (2017). *Revisiting unreasonable effectiveness of data in deep learning era*. [arXiv:1707.02968 [cs]].

[46] Banko, M., Brill, E. (2001). Mitigating the paucity-of-data problem: Exploring the effect of training corpus size on classifier performance for natural language processing. In *Proceedings of the First International Conference on Human Language Technology Research*.

[47] Abadi, M., Agarwal, A., Barham, P., Brevdo, E., Chen, Z., Citro, C., Corrado, G.S., Davis, A., Dean, J., Devin, M., Ghemawat, S., Goodfellow, I., Harp, A., Irving, G., Isard, M., Jia, Y., Jozefowicz, R., Kaiser, L., Kudlur, M., Levenberg, J., Mañé, D., Monga, R., Moore, S., Murray, D., Olah, C., Schuster, M., Shlens, J., Steiner, B., Sutskever, I., Talwar, K., Tucker, P., Van-Houcke, V., Vasudevan, V., Végas, F., Vinyals, O., Warden, P., Wattenberg, M., Wicke, M., Yu, Y., Zheng, X. (2015). *TensorFlow: Large-scale machine-learning on heterogeneous systems*. Software available from: tensorflow.org

[48] Buduma, N., Locascio, N. (2017). *Fundamentals of deep learning: designing next-generation machine intelligence algorithms*. O'Reilly Media.

[49] Ketkar, N. (2017). *Deep learning with Python: a hands-on introduction*. Apress.

[50] Ruder, S. (2016), *An overview of gradient descent optimization algorithms..* [arXiv:1609.04747 [cs]]. Comment: Added derivations of AdaMax and Nadam.

[51] Boughorbel, S., Jarray, F., El-Anbari, M. (2017). Optimal classifier for imbalanced data using Matthews Correlation Coefficient metric. *PLOS ONE*, **12** (6).